BIONATURE 2013

The Fourth International Conference on Bioenvironment, Biodiversity and Renewable Energies

ISBN: 978-1-61208-261-5

March 24 - 29, 2013

Lisbon, Portugal

BIONATURE 2013 Editors

Son V. Nghiem, Jet Propulsion Laboratory / California Institute of Technology - Pasadena, USA

BIONATURE 2013

Foreword

The Fourth International Conference on Bioenvironment, Biodiversity and Renewable Energies [BIONATURE 2013], held between March 24 - 29, 2013 in Lisbon, Portugal, covered these two main areas: environment and renewable and sustainable energies.

Environmental change awareness is a key state of spirit and legislation for preventing, protecting, and ultimately saving the planet biodiversity. Technical and practical methods for applying bio-agriculture for the public's health and safety are primary targets. The goal is the use of ecological economic stimuli in tandem with social and governmental actions preventing deforestation, pollution, and global warming. To cope with the climate and landscape changes advanced technical inventory of tools and statistics on lessons learned are needed to derive appropriate measure and plan accordingly.

Replacing the classical energy with alternative renewable energy (green energy), such as bioenergy, eolian energy, or solar energy is an ecological and economic trend that suggests important socio-economic advantages: using native renewable resources, increasing of self-sufficiency rate of energy and promoting use of clean energy, and that way, polluting emissions to the air will be reduced. Bioenergy is renewable energy derived from biological sources, to be used for heat, electricity, or vehicle fuel. Biofuel derived from plant materials is among the most rapidly growing renewable energy technologies. In several countries corn-based ethanol is currently the largest source of biofuel as a gasoline substitute or additive. Recent energy legislation mandates further growth of both corn-based and advanced biofuels from other sources. Growing biofuel demand has implications for U.S. and world agriculture. Eolian energy is currently used throughout the world on a large scale. In the past decade, its evolution shows its acceptance as a source of generation, with expressive growth trends in the energy matrices in the countries where this source is used Eolian energy is renewable and has very low environmental impact. To generate it, there are no gas emissions, no effluent refuse, and no other natural resources, such as water, are consumed. Photovoltaic technology makes use of the energy in the sun, and it has little impact on the environment. Photovoltaics can be used in a wide range of products, from small consumer items to large commercial solar electric systems. The event brought together the challenging technical and regulation aspects for supporting and producing renewable energy with less or no impact on the ecosystems. There are several technical integration barriers and steps for social adoption and governmental legislation to favor and encourage this kind of energy.

We take here the opportunity to warmly thank all the members of the BIONATURE 2013 Technical Program Committee, as well as the numerous reviewers. The creation of such a high quality conference program would not have been possible without their involvement. We also kindly thank all the authors who dedicated much of their time and efforts to contribute to BIONATURE 2013. We truly believe that, thanks to all these efforts, the final conference program consisted of top quality contributions.

Also, this event could not have been a reality without the support of many individuals, organizations, and sponsors. We are grateful to the members of the BIONATURE 2013

organizing committee for their help in handling the logistics and for their work to make this professional meeting a success.

We hope that BIONATURE 2013 was a successful international forum for the exchange of ideas and results between academia and industry and for the promotion of progress in the fields of bioenvironment and renewable energies.

We are convinced that the participants found the event useful and communications very open. We also hope the attendees enjoyed the charm of Lisbon, Portugal.

BIONATURE 2013 Chairs:

Son V. Nghiem, Jet Propulsion Laboratory / California Institute of Technology - Pasadena, USA
Suhkneung Pyo, Sungkyunkwan University - Suwon City, South Korea

BIONATURE 2013

Committee

BIONATURE Advisory Chairs

Son V. Nghiem, Jet Propulsion Laboratory / California Institute of Technology - Pasadena, USA
Suhkneung Pyo, Sungkyunkwan University - Suwon City, South Korea

BIONATURE 2013 Technical Program Committee

Dhrubes Biswas, Indian Institute of Technology, India
Rupp Carriveau, Union Gas / University of Windsor University of Windsor, Canada
Longjian Chen, China Agricultural University, China
Gianfranco Chicco, Politecnico di Torino, Italy
Hany A. El-Shemy, Cairo University - Giza, Egypt
Jerekias Gandure, University of Botswana, Botswana
Josean Garrués Irurzun, University of Granada, Spain
Giuseppe Genon, Politecnico di Torino, Italy
Bassim H. Hameed, University of Science Malaysia - Penang, Malaysia
Kathleen Hefferon, Cornell University, USA
Iem Heng, NYC College of Technology/CUNY – Brookly, USA
Ana Jesús López, University of Oviedo, Spain
Man Kee Lam, Universiti Sains Malaysia - Penang, Malaysia
Yu-Te Liao, National Chung-Cheng University, Taiwan
Valentinas Klevas, Kaunas University of Technology / Lithuanian Energy Institute, Lithuania
Villy Kourafalou, University of Miami/ Rosenstiel School of Marine and Atmospheric Science, USA
Blanca Moreno Cuartas, University of Oviedo, Spain
Ali Mostafaeipour, Yazd University, Iran
Abdeen Mustafa Omer, Energy Research Institute (ERI) - Khartoum, Sudan
Son V. Nghiem, Jet Propulsion Laboratory / California Institute of Technology - Pasadena, USA
Patrícia Pereira da Silva, University of Coimbra & INESC-Coimbra, Portugal
Suhkneung Pyo, Sungkyunkwan University - South Korea
Bale V. Reddy, University of Ontario Institute of Technology - Oshawa, Canada
Francisca Segura Manzano, University of Huelva, Spain
Elena Serrano, University of Alicante, Spain
Atul Sharma, Rajiv Gandhi Institute of Petroluem Technology - Rae Bareli, India
Vladimir Strezov, Macquarie University - Sydney Australia
Lee Keat Teong, Universiti Sains Malaysia - Penang, Malaysia
Mihaela Ulieru, The University of New Brunswick - Fredericton, Canada
Talal Yusaf, University of Southern Queensland - Toowoomba, Australia
Victor Zaichenko, Biocenter, Russia

Copyright Information

For your reference, this is the text governing the copyright release for material published by IARIA.

The copyright release is a transfer of publication rights, which allows IARIA and its partners to drive the dissemination of the published material. This allows IARIA to give articles increased visibility via distribution, inclusion in libraries, and arrangements for submission to indexes.

I, the undersigned, declare that the article is original, and that I represent the authors of this article in the copyright release matters. If this work has been done as work-for-hire, I have obtained all necessary clearances to execute a copyright release. I hereby irrevocably transfer exclusive copyright for this material to IARIA. I give IARIA permission or reproduce the work in any media format such as, but not limited to, print, digital, or electronic. I give IARIA permission to distribute the materials without restriction to any institutions or individuals. I give IARIA permission to submit the work for inclusion in article repositories as IARIA sees fit.

I, the undersigned, declare that to the best of my knowledge, the article is does not contain libelous or otherwise unlawful contents or invading the right of privacy or infringing on a proprietary right.

Following the copyright release, any circulated version of the article must bear the copyright notice and any header and footer information that IARIA applies to the published article.

IARIA grants royalty-free permission to the authors to disseminate the work, under the above provisions, for any academic, commercial, or industrial use. IARIA grants royalty-free permission to any individuals or institutions to make the article available electronically, online, or in print.

IARIA acknowledges that rights to any algorithm, process, procedure, apparatus, or articles of manufacture remain with the authors and their employers.

I, the undersigned, understand that IARIA will not be liable, in contract, tort (including, without limitation, negligence), pre-contract or other representations (other than fraudulent misrepresentations) or otherwise in connection with the publication of my work.

Exception to the above is made for work-for-hire performed while employed by the government. In that case, copyright to the material remains with the said government. The rightful owners (authors and government entity) grant unlimited and unrestricted permission to IARIA, IARIA's contractors, and IARIA's partners to further distribute the work.

Table of Contents

South Russia Steppe Forests: Features and Problems

Maria Kryzhevich (Martynova)
Southern Federal University
SFU
Rostov-on-Don, Russia
e-mail: maymars@mail.ru

***Abstract* – Extrazonal steppe forests are studied. In this paper we consider Rostov region which is a typical steppe area, where the majority of forests are man-made. We aim to analyze the present state of steppe forest landscapes and to discuss some related geo-environmental problems. Damage caused by fires, pests, diseases and unbalanced forestry is estimated for forest ecosystems of South Russia.**

Keywords – extrazonal landscapes; steppe forests; forest fires; grassland fires; man-made forests.

I. INTRODUCTION

Steppe summergreen forests are extrazonal, this landscape forms ecological framework of the territory. According to botanical and geographical zoning, studied area belongs to the Eurasian steppe region, the Black Sea province, and the Azov-Black Sea subprovince [1, 2]. The main part of Russian steppe forests is man-made. These landscapes perform a lot of ecological functions: gas-forming, climate, wind protection, conservation, agricultural and so on. The ecological troubles of these landscapes are caused by non-comfortable environmental conditions and by high density of the population of the region. In this paper we give a survey of the contemporary state of steppe forest and describe some reasons of existing troubles.

This article includes six sections and three figures.

In Section II, the main purpose of the research is mentioned and the methods we used have been referred. Conditions, typical for the steppe area of Southern Russia, are described in Section III. In Section IV, we provide a zoning of forests of the area and study their current characteristics. In Section V, the main result of the paper is provided; statistical observation for fire risks according areas of the region is given. Conclusion is provided in Section VI.

II. PURPOSE AND METHODS

The purpose of this investigation is to analyze the current status and major geo-environmental problems of an important component of zonal steppe landscapes – the forest. Forest zones play an exclusive role in ecological balance of Southern Russia because these lands are sparsely wooded and significantly populated. The density of population in Rostov region is 42.2 pers. / Sq km while the average one for Russian Federation is 8.4 pers. per Sq km only. An original forestry zoning including geographic structure of Southern Russia forest fires has already been made by author [4]. In this paper, we refresh and precise this zoning using modern data.

Several expeditions have been performed in 2001-2011 in order to study state of woodlands. The data obtained by region monitoring during 1960-2011 have been summarized. Field, statistical and cartographic methods have been actively used.

III. PRINCIPAL PARAMETERS OF STEPPE FORESTS

Rostov region is a steppe area. It has a plane platform geological structure with a developed river valley systems and three zonal landscapes types: true (bunchgrass) steppe, dry steppe and desert type steppe (Figure 1).

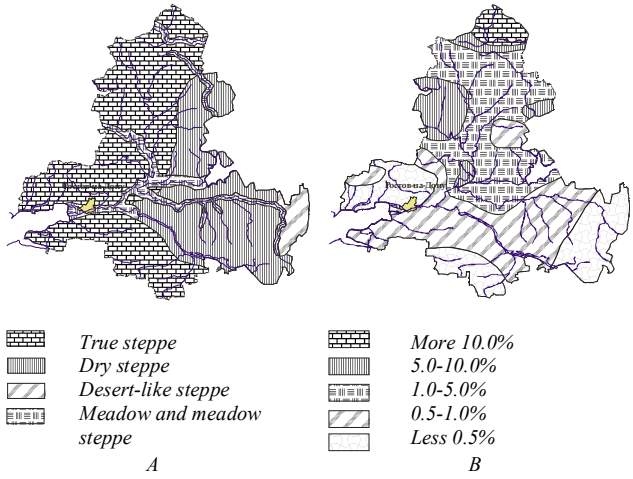

Figure 1. Natural landscape types of Rostov Region (A) and forest coverage of this region (B).

Meadows and meadow steep are intrazonal landscapes. The principal factor that limits the forest vegetation growth is environmental humidity.

Steppe landscapes are characterized by arid hot summers (+22/24°C), moderately cold winters (-5/-9°C), and some negative forest-grown factors: low relative humidity, large temperature amplitude fluctuations, agricultural drought, extremely high summer temperatures and strong dry eastern winds. Mean annual precipitation is about 530-550 mm in the southwest and 320-360 mm – in the southeast of this

 ISBN: 978-1-61208-261-5

territory [3]. Maximum precipitation occurrence is recorded in the warm season – the growing season.

Bunchgrass steppe (with normal forest coverage about 3.0%) is characterized by a medium humidity coefficient (more than 4.1), dry steppe (1.7%) has a reduced index (3.5–4.0) and desert type steppe has a low index (less than 3.4).

IV. INVESTIGATIONS

The majority of boreal steppe forests are man-made. There are contrasting woods with different conditions. The main part of this framework is floodplain forest. A big part of Lower Don forests is inundated, sometimes naturally and sometimes artificially. These landscapes are poorly preserved. There are 425 species of plants, including 225 species of forest flora [4]. Typically, these landscapes have a high biological age, a stratiness loss. Their ecological functions, the stability have been reduced, the vegetation has adversely changed. Some environmental factors contribute to the spread of forest and grassland fires. The conditions of these forests have been violated after Tsimlyansky reservoir on the river Don was constructed.

Ravine forests represent another woodland type of this region. The area is richer in species. There are 592 species of plants, including 292 species of forest flora [2]. The main tree species are *Quércus róbur* (32%), *Pínus sylvéstris* (31% of the forest area), *poplars* (9%), *Robínia pseudoacácia* and others (Figure 2).

Also, sandy, so-called «arennye» forests are there. Reforestation works yield to appearance of man-made pine forests. Some aspen and the birch wood lots are remained fragments of natural forests.

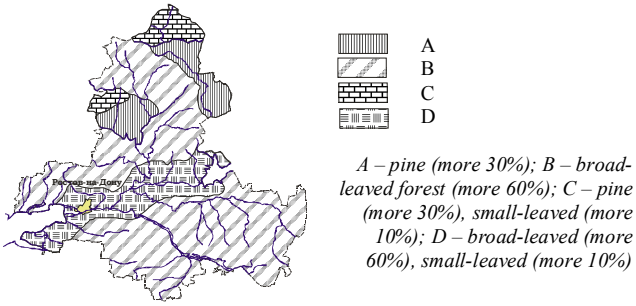

A – pine (more 30%); B – broad-leaved forest (more 60%); C – pine (more 30%), small-leaved (more 10%); D – broad-leaved (more 60%), small-leaved (more 10%)

Figure 2. Main tree species of Rostov forests.

All forests perform a protective function. According to Russian classification 52.1% of them are steppe and desert type forests; 18.2% are anti-erosion and gully-stabilization; 6.7% are bank-protection forests, 1.6% are «green areas»; 2.7% are «urban forests» and so on.

The following problems are crucial for considered landscapes: senescence of trees, appearance of dead wood areas, reduction of ecological performance, and, of course, forest fires. The steppe woodland has the highest fire danger class in Southern Russia (2.2). Forests of the first and the second forest class of fire danger cover 58% of regional forest area [5, 6]. Moreover, line field-protection forests are mono-breed (*Pínus sylvéstris)* woodlands mostly planted in 1950-1960.

Unfortunately, the juridical status of these forests is not specified and, actually, nobody is responsible for their protection. The disastrous grassland fires are typical for this area (Figure 3).

V. MAIN RESULTS

As a result of field and statistical observations, 7 levels of fire danger have been specified. There are areas of 2nd, 5th a 6th level inside the Rostov agglomeration. A medium and sometimes even relatively high ecological potential of the landscapes (12.0-16.0 or more [7, 8]) is proper for this area while the forest coverage is reduced there (1.5-2.5%). Mainly, the oak forests are represented. Large and medium forest fires are not typical for this region [9].

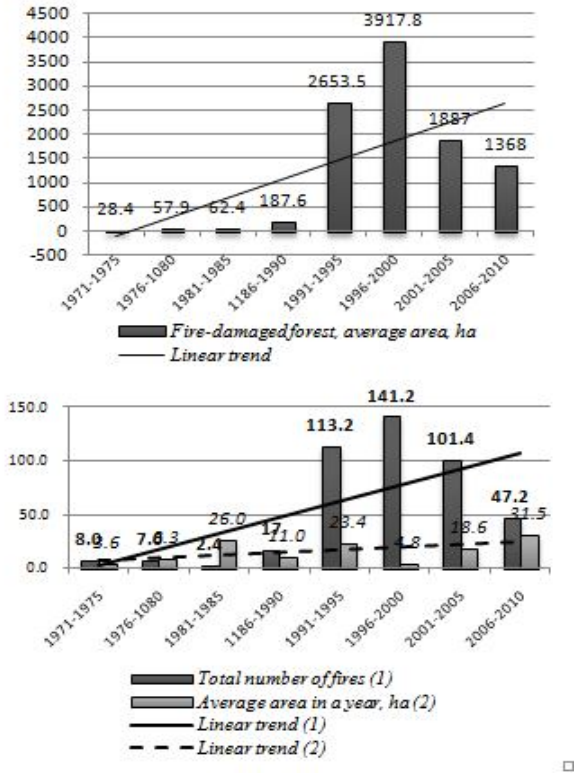

Figure 3. Dynamics of wood burning indicators of Rostov forests during the period from1971 to 2010.

Many forest fires occur near populated areas in field-protection forests. Both the forest coverage and the number of forest fires increase during last 30 years (Figure 2). However, nowadays forest fires in near-Rostov area are localized. Unfortunately, the artificial grassland fire is the principal reason of disasters. The proportion of crown fires is quite high (50% in 2007, about 30 in 2008, 75% in 2010). This is very destructive for the steppe forests, as natural

 ISBN: 978-1-61208-261-5

forest regeneration is almost impossible. The years 2003, 2004, 2007-2011 correspond to peak values of fires. Mostly, there were simple natural reasons for this. Hot, dry and windy weather contributed intensive spread of the fire. The situation is deteriorates by high density of the recreational facilities, farms and roads.

We expect to continue the expedition activity in order to find out trends of forest development, describe areas affected by fire and related damages. The findings of this paper and ones of the following researches may be used for future forest recovery works in damaged areas.

VI. CONCLUSION

Frequent natural cataclysms of recent years and unbalanced forestry caused additional load on steppe forests. They started losing natural layering. The total area of inundated, infected and burnt forests increased. Meanwhile, the natural recovering is almost impossible for such type of forests. This may lead to loss of this unique landscape.

We expect to continue the expedition activity in order to find out trends of forest development, describe areas affected by fire and related damages.

The author thanks all anonymous reviewers for interesting and useful remarks and comments.

REFERENCES

[1] S. Gribova, T. Isachenko, and E. Lavrenko, The vegetation of the European USSR. Leningrad, 1980.

[2] Plant resources. Natural resources of the North Caucasus. Part 1. Forest. Rostov-on-Don, 1980.

[3] T. Smagina and V. Kutilin, “Anthropogenic transformation of Rostov region natural landscapes” Ecological and geographical Bulletin of Southern Russia, May. 2002. no 2, pp. 33-41 (in Russian).

[4] M. Martynova, “Forest zoning in the open steppe” Lesnoe hozyaystvo, Aug. 2004. no. 4, pp. 21-22 (in Russian).

[5] A. Isachenko, Introduction to environmental geography. St. Petersburg, 2003.

[6] M. Martynova, Features of Rostov region forest fire regime. Proc. Conference Structural and functional forests dynamics organization. Krasnoyarsk, Sep., 2004.

[7] M. Martynova, Geoecology. Geosystems optimization. Rostov-on-Don, 2009.

[8] G. Zozulin, The Lower Don forests. Rostov-on-Don, 1992.

[9] B. Gorbachev, Vegetation and natural forage lands of the Rostov region. Rostov-on-Don, 1980.

 ISBN: 978-1-61208-261-5

Arctic Sea Ice Reduction and Tropospheric Chemical Processes

S. V. Nghiem[1], P. B. Shepson[2], W. Simpson[3], D. K. Perovich[4], M. Sturm[5], T. Douglas[5], I. G. Rigor[6], P. Clemente-Colón[7], J. P. Burrows[8,9], A. Richter[8], A. Steffen[10], R. Staebler[10], D. Obrist[11], C. Moore[11], J. Bottenheim[10, retired], U. Platt[12], D. Pöhler[12], S. General[12], J. Zielcke[12], J. D. Fuentes[13], D. K. Hall[14], L. Kaleschke[15], J. Woods[16], C. Hager[16], J. Smith[16], C. R. Sweet[16], K. Pratt[2], K. Custard[2], P. Peterson[3], S. Walsh[3], E. Gleason[3], E. Saiet[3], M. Webster[6], R. Lieb-Lappen[17], C. Linder[6], and G. Neumann[1]

[1]Jet Propulsion Laboratory, California Institute of Technology, Pasadena, California, U.S.A.
[2]Departments of Chemistry and Earth and Atmospheric Sciences, Purdue University, Lafayette, Indiana, U.S.A.
[3]Department of Chemistry, University of Alaska Fairbanks, Fairbanks, Alaska, U.S.A.
[4]U.S. Army Cold Regions Research and Engineering Laboratory, Hanover, New Hampshire, U.S.A.
[5]U.S. Army Cold Regions Research and Engineering Laboratory, Fairbanks, Alaska, U.S.A.
[6]Polar Science Center, Applied Physics Laboratory, University of Washington, Seattle, Washington, U.S.A.
[7]National Oceanic and Atmospheric Administration, National Ice Center, Washington, District of Colombia, U.S.A.
[8]Institute of Environmental Physics, University of Bremen, Bremen, Germany
[9]Biogeochemistry Programme, NERC Centre for Ecology and Hydrology, Wallingtonford, Oxfordshire, U.K.
[10]Science and Technology Branch, Environment Canada, Toronto, ON, Canada
[11]Division of Atmospheric Sciences, Desert Research Institute, Reno, Nevada, U.S.A.
[12]Institute for Environmental Physics, University of Heidelberg, Heidelberg, Germany
[13]Department of Meteorology, Penn State, University Park, Pennsylvania, U.S.A.
[14]NASA Goddard Space Flight Center, Greenbelt, Maryland, U.S.A.
[15]Institute of Oceanography, University of Hamburg, Hamburg, Germany
[16]U.S. Naval Academy, Annapolis, Maryland, U.S.A.
[17]Dartmouth College, Hanover, New Hampshire, U.S.A.
Contact e-mail: Son.V.Nghiem@jpl.nasa.gov

Abstract—**Arctic sea ice extent reached another historical record low in summer 2012. More importantly, perennial sea ice extent in 2012 set the new record low in the long period that extends back to the last half of the 20th century as observed by a combination of long-term measurements acquired by ocean buoys and decadal data acquired by satellite scatterometers. To investigate impacts of sea ice reduction on atmospheric chemical processes, we conducted the BRomine, Ozone, and Mercury EXperiment (BROMEX) in March-April 2012 around Barrow, Alaska. We present an overview of BROMEX and highlight results to document sea ice change and chemical processes. We found a large number of bromine explosion events occurred in the BROMEX area where seasonal sea ice dominated.**

Keywords-Arctic sea ice; bromine; ozone; mercury; BROMEX.

I. INTRODUCTION AND OBJECTIVE

In the context of Arctic change in the last half century, perennial sea ice, the class of thicker and older ice important to the stability of Arctic sea ice, has been declining most precipitously in the last decade. Nghiem et al. [1] reported the extent of perennial ice in the month of March (1950s to the 2000s), estimated by the buoy-based Drift-Age Model (DM) together with nearly a decade of QuikSCAT (QS) satellite observations within the domain of the DM (excluding peripheral seas such as Greenland Sea and the Canadian Arctic Archipelago). From the published data [1], perennial ice extent declined at rate of 0.5 million km^2 per decade in the 1970s-1990s while there was no discernable trend in the 1950s-1960s. Abruptly, the rate of decrease has tripled to 1.5 million km^2 per decade in the 2000s. Such rapid reduction has resulted in a regime shift of Arctic sea ice to being dominated by seasonal sea ice that grows and melts annually. The springtime distribution of these ice classes is critical in terms of preconditioning prior to the summer melt, and moreover it plays a major role in tropospheric chemical processes controlling bromine, ozone, and mercury photochemistry in the Arctic atmospheric boundary layer. To investigate impacts of sea ice reduction on atmospheric halogen and other chemical processes, we conducted the BRomine, Ozone, and Mercury EXperiment (BROMEX) in March-April 2012 around Barrow, Alaska, which was successfully carried out. In the sections below, we state the science issues (II), describe BROMEX (III), present the observations (IV), and provide the summary (V).

II. SCIENCE ISSUES

Observations of the state of Arctic sea ice using multiple satellites show drastic loss of perennial ice extent [1]. More importantly, an initial study has led to the first report of BrO in a clear vortex pattern, and a discovery of an apparent topographic control on the transport and distribution processes of bromine monoxide (BrO) [2]. The full field of the three-dimensional rising-air-parcel (RAP) model [2] forced by the NCEP/NCAR reanalysis [3] consistently reproduces the spatial pattern of BrO observed by the Global Ozone Monitoring 2 (GOME-2) satellite [4].

 ISBN: 978-1-61208-261-5

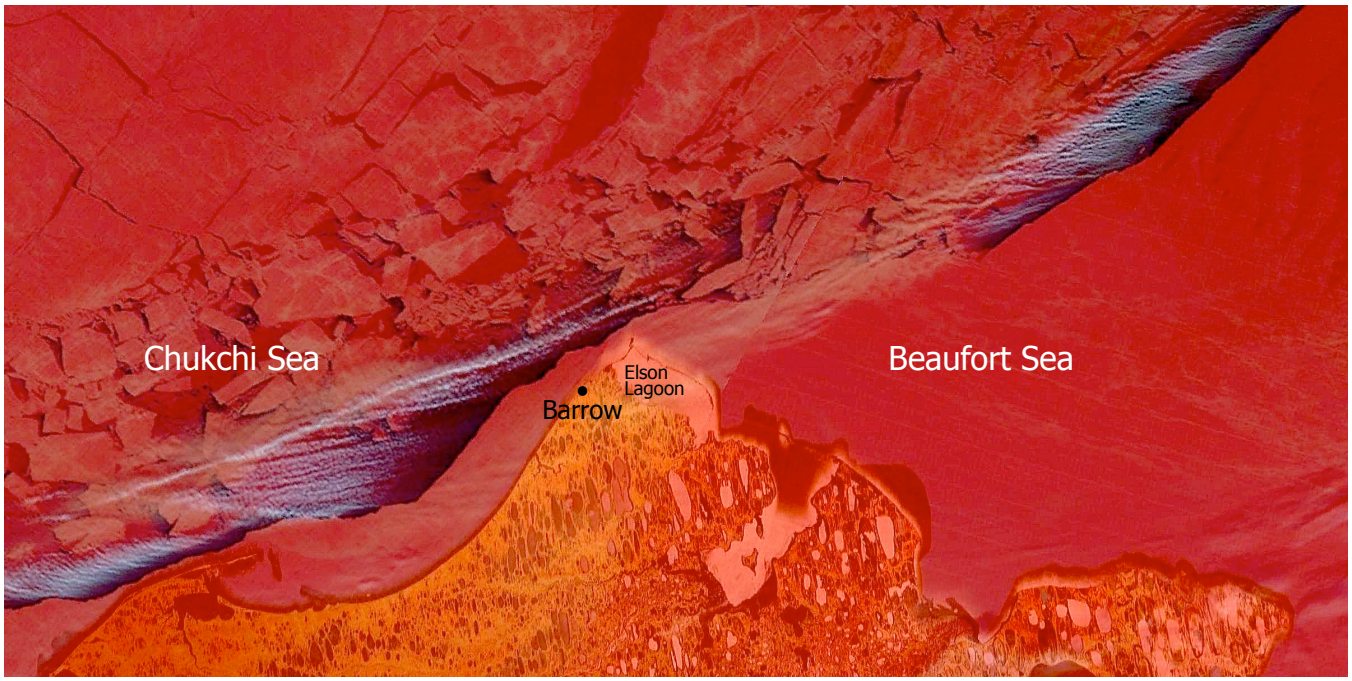

Figure 1. Image from a composition of bands 3, 6, and 7 acquired by the MODIS Terra satellite on 24 March 2012. Sea ice in the Chukchi Sea and the Beaufort Sea appears as red. Dark areas in the ocean are leads, formed by wind forcing that ruptured the sea ice cover. Grayish streaks are vapor plumes emanating from the leads. Landscape features are seen through the translucently overlain MODIS image with red-orange shades indicating snow cover.

The bromine explosion process is briefly summarized here. At the polar-sunrise time, gaseous bromine (Br_2) is photo-dissociated into Br atoms, which catalytically destroy ozone (O_3) and oxidize gaseous element mercury (GEM) with the Br atoms being regenerated in excess in this autocatalytic process. Hypobromous acid (HOBr) formed in a termination step deposits to saline surfaces, generating Br_2 that evolves to the gas phase, providing twice as many Br atoms back to the gas phase, and hence the term "bromine explosion" is used to describe this behavior [5].

Despite recent advances in understanding Arctic tropospheric halogen chemistry in the context of a changing state of Arctic sea ice, key science questions still remain to be answered in order to understand the impact of the recent drastic reduction of Arctic sea ice, such as how the bromine is initiated, recycled, transported, and terminated. Sea ice reduction has profoundly changed the Arctic environment and halogen chemical processes involved in the bromine explosion, ozone depletion, and mercury deposition events. This is a cascade of photochemical reactions that abruptly increase gaseous bromine such as bromine monoxide (BrO) in the atmospheric boundary layer, leading to the depletion of tropospheric ozone (O_3), and the oxidation of gaseous elementary mercury (GEM) to a reactive form that deposits onto land, ice, and ocean surfaces in the Arctic.

III. THE BROMEX FIELD CAMPAIGN

BROMEX was conducted in March and April 2012 around Barrow, Alaska (Figure 1). The field area extended from inland terrestrial sites to a large region of the sea ice offshore, where energetic dynamics created large leads, fortuitously providing a variety of sea ice and atmospheric conditions for this investigation. BROMEX included participation and contributions from more than thirty scientists, researchers, and support staff from multiple international institutions.

We coordinated and collected satellite data, including a number of near-real-time products, from multiple satellite instruments. These include the Moderate Resolution Imaging Spectroradiometer (MODIS), the Advanced Microwave Scanning Radiometer on the Earth Observing System (AMSR-E), the Special Sensor Microwave Imager/ Sounder (SSMIS), GOME-2, the Scanning Imaging Absorption Spectrometer for Atmospheric Cartography (SCIAMACHY), the Ozone Monitoring Instrument (OMI), the RADARSAT-2 Synthetic Aperture Radar (SAR), the Envisat Advanced SAR, the TerraSAR-X add-on for Digital Elevation Measurements (TanDEM-X) SAR, the Soil Moisture and Ocean Salinity (SMOS) radiometer, the CryoSat-2 altimeter, and the Oceansat-2 scatterometer. Multiple products derived from satellite data by the Jet Propulsion Laboratory (JPL), NASA Goddard Space Flight Center (GSFC), U.S. National Ice Center (NIC), University of Bremen, and University of Hamburg were used to plan for and to support the BROMEX campaign.

Three different aircraft were used for instrument deployments and data collections. We deployed atmospheric chemical and meteorological buoys in the Chukchi Sea and the Beaufort Sea. We set up instruments to measure multiple chemical species of mercury at sites on sea ice and on land. In addition to existing weather stations, we installed a meteorological tower and a snow measurement tower at a site on the tundra. At these sites, continuous atmospheric chemical and meteorological measurements were made for many weeks.

 ISBN: 978-1-61208-261-5

We made measurements and collected samples of sea ice, snow, seawater, and air for physical, meteorological, chemical, biological, and acoustic studies. We obtained an enormous amount of satellite and field data. In the sections below, we present the BROMEX measurement components and discuss highlights of the results to document sea ice change and observed atmospheric and snow chemical processes.

IV. SATELLITE, ARICRAFT, AND FIELD OBSERVATIONS

A. Satellite Observations

Arctic sea ice extent reached another historical record low in summer 2012. More importantly, perennial sea ice extent in 2012 set the new record low in the extensive period from the last half of the 20th century up to date, as observed by a combination of long-term measurements acquired by ocean buoys and decadal data acquired by satellite scatterometers. The NASA SeaWinds scatterometer mission with the QuikSCAT (QS) satellite acquired the most stable and accurate Ku-band backscatter data [6] over a decade (1999-2009). The Oceansat-2 (OS2) scatterometer [7] launched by the Indian Space Research Organisation (ISRO) in September 2009 continues the scatterometer data collection to the present. The satellite data were used to identify, map, and monitor perennial sea ice versus seasonal sea ice that grows and melts annually [1]. To monitor winter perennial and seasonal sea ice, the DM [8] provides over a half-century estimate of Arctic sea ice age distribution to determine the long-term trend since 1955. From monthly gridded fields of ice motion based on buoy data, this model estimates sea ice age, and thereby identifies perennial and seasonal sea ice. In the DM spatial domain, model estimates and satellite scatterometers consistently determined the three-fold decrease rate of perennial sea ice extent in the 2000s.

Updated data from OS2 indicated that springtime perennial sea ice extent reached a new low record in 2012. Except for a narrow band of perennial sea ice in the north of the Alaskan coast, seasonal sea ice dominated the sea ice cover in the Chukchi Sea and the Beaufort Sea. The thinner and weaker seasonal ice, compared to perennial ice, facilitates the formation of large leads when strong winds force sea ice away from shore and creates long open water areas that quickly refreeze and support the growth of new (nilas) ice and frost flowers on the new sea ice surface. This new ice is highly saline and provides a potential source for lower atmospheric halogen chemical reactions. Figure 1, a MODIS image acquired on 24 Mach 2012 during BROMEX, shows a large lead in the Chukchi Sea to the west of Barrow. On the same day, both GOME-2 and OMI satellites detected extensive areas where a bromine explosion occurred above the ocean and across the terrestrial tundra land in the North Slope of Alaska.

B. Aircraft Observations

During BROMEX in March 2012, the Purdue Airborne Laboratory for Atmospheric Research (ALAR; see details at [9]) was used as a key platform to measure ozone (O_3, in-situ), BrO (produced entirely from Br atoms reacted with O_3, with Multi Axis – Differential Optical Absorption Spectroscopy or MAX-DOAS), and aerosol number and size distributions (in-situ). Eleven flights were conducted over continuous first-year sea ice in the Beaufort Sea, over new ice and leads with frost flower coverage in the Chukchi Sea, and over the snow-covered tundra between Barrow, Deadhorse, and the Brooks Range. All systems performed well during this campaign.

From initial analyses of the ALAR data, a number of interesting findings were apparent during the flights. For example, on 24 March 2012, we flew over the tundra, at a constant altitude, and observed the BrO distribution in the boundary layer. There was a relatively enhanced column of BrO over the tundra on this day. On other days, elevated aerosol layers were observed aloft, possibly suggesting long-range transport. Interestingly, on two flights, we observed deeper ozone depletions over the tundra, compared to the sea ice. Overall, the simultaneous O_3, BrO, and aerosol measurements will yield many insights into halogen cycling.

Through a coordination with the NASA IceBridge program, the NASA P3 aircraft was flown across the BROMEX field domain from the Beaufort Sea, across Elson Lagoon and the North Slope tundra, to the Chukchi Sea. Sensors on the IceBridge P3 aircraft measured multiple parameters including: sea ice thickness, snow thickness, surface height, and surface temperature. These parameters are useful for interpretation of sea ice and snow physical properties and for investigating their roles in halogen photochemical processes.

C. Field Observations

Field activities for BROMEX were focused on two types of locations: (1) buoy sites in the Arctic Ocean, and (2) snowmobile-accessible locations on land and shore-fast sea ice near Barrow, Alaska. A major goal of the near-shore sea ice work was to access a location where the landfast ice and pack ice meet so that when a major flaw lead opened we would have access to the open water. A safety plan was carefully developed and implemented for BROMEX since this area could be dynamic and frequented by polar bears.

A key component of BROMEX was the deployment of two chemistry buoys, fabricated by the University of Alaska Fairbanks (UAF): IceLander 1 (IL1) in the Beaufort Sea and IceLander 2 (IL2) in the Chukchi Sea. This deployment process had three steps: (1) defining the criteria for a suitable floe, (2) analyzing remote sensing imagery to select candidate floes, and (3) flying out to the candidate floes for an in-situ evaluation. The criteria were: first-year ice, center area of hundreds of meters without major ridges, snow covered, accessible by helicopter, and likely to survive into the melt season. With the high quality satellite imagery, the U.S. Army Cold Regions Research and Engineering Laboratory (CRREL) and UAF easily found the candidate floes and selected the best floe to deploy the IceLanders. Surveys of snow depths were performed, and results showed that average snow depths were comparable at the two sites.

IL1 was stationary until its retrieval in March 2012. IL2 drifted across sea ice under a variety of conditions from pack ice, to lead opening and closing, and unconsolidated sea ice in March to June 2012 when it was knocked over by

 ISBN: 978-1-61208-261-5

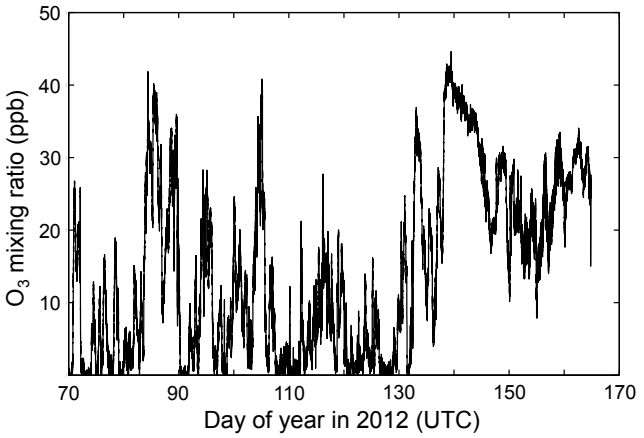

Figure 2. Ozone mixing ratio from IceLander 2 in the Chukchi Sea. Many ozone depletion events were observed in March to May 2012.

a polar bear. An identical DOAS system was also installed at a building in Barrow (BRWDOAS), which has been operating continuously to the present. An analysis has been completed for Level-2 (slant column density of gases versus elevation angle) data and also Level-3 (vertical profiles of BrO) data for BRWDOAS, IL1, and IL2. O_3 data were processed and finalized for IL1, IL2, and BRWDOAS. IL2 O_3 in Figure 2 revealed that ozone depletion events occurred frequently forcing O_3 level to near complete depletion in many instances in the Chukchi Sea region off the west coast of Barrow where it was dominated by seasonal sea ice. A preliminary analysis has been carried out for Lagrangian matching of data between IL1, IL2, and Barrow to look for changes in BrO and ozone related to sea ice. First examinations indicate that ozone and BrO changes between sites are small. An examination of the longer-term seasonal behavior of IL2 and BRWDOAS revealed a relationship between the BrO seasonal end date and snow properties. Additionally, snow microphysics is currently researched to obtain a solid interpretation of these observations.

To assess how changing sea ice conditions may affect the regional cycling of atmospheric mercury, Environment Canada's Out On the Ice (OOTI) system was deployed and operated at a site approximately 1 km from shore on the frozen Arctic Ocean during March-April 2012. This system measured speciated atmospheric mercury concentrations, including gaseous elemental mercury (GEM), reactive gaseous mercury (RGM), and fine particulate bound mercury (FPM). Environment Canada and the Desert Research Institute also collected data for surface-atmosphere fluxes of GEM and O_3, and meteorological variables, and measured speciated atmospheric mercury and O_3 concentrations at a second site 5 km inland in the Arctic tundra, co-located with in-situ halogen measurements by Purdue University. At each site, surface snow samples and a sample from a newly designed cold-plate sampler were collected daily for total mercury and major ion concentrations. Striking changes in GEM, RGM, and FPM concentrations occurred during the transition from a large open lead to newly frozen sea ice, furthering our understanding of the complexity of Arctic mercury depletion. The concentration of GEM was different at the inland tundra site and at the OOTI site over the sea ice reflecting the impact of sea ice on the mercury cycling.

At the inland tundra site, chemical ionization mass spectrometry was utilized to measure the concentrations of various bromine species, including Br_2, HOBr, and BrO, at a high temporal resolution. Together with co-located measurements of ozone and mercury, these ambient halogen measurements are being utilized to gain greater insights into the role of bromine in ozone and mercury depletion events. In addition, these BrO measurements on the tundra are being compared with other BrO measurements completed at other locations. Overall, a good agreement has been observed between the DOAS and chemical ionization mass spectrometry measurements of BrO. For the first time, collocated simultaneous mercury speciation and in situ halogen measurements were made to understand the link between these atmospheric components.

Accurate estimates of wind and temperature are required for understanding the myriad of processes involved in the transport and distribution of the chemicals. In-situ observations were provided by nearby National Oceanic and Atmospheric Administration (NOAA) weather stations, and to accurately document conditions at each field site, portable weather stations (PWS) were installed at each site. The Applied Physics Laboratory of the University of Washington (APL/UW) provided the PWS at the tundra site, and deployed buoys from the International Arctic Buoy Programme (IABP) offshore from the field camp to assure that there were adequate measurements for the analyzed weather fields produced by the National Weather Service (NWS), Alaska Weather Research Forecasts (WRF), and the National Centers for Environment Prediction (NCEP) reanalysis fields. Moreover, ten thermochrons provided by GSFC were deployed in different sea ice, snow, and built environments for comparison with MODIS satellite data collocated in time and in space with the surface measurements. Initial results revealed complexities that call for a rigorous protocol to be developed for accurate and consistent temperature measurements.

Understanding the role of snow in the chemical processes is crucial. During BROMEX, intensive fieldwork was carried out to document snow conditions around Barrow and under the flight line of the IceBridge P3 aircraft. The mean snow depth measured by the P3 aircraft was validated with thousands of snow depth measurements collected on sea ice and tundra. Overall, about 10,000 snow measurement samples were obtained across the BROMEX domain. The initial interpretation of the results suggests the P3 measurements appear to overestimate areas of low snow cover, and underestimate areas of high snow cover. To investigate the change in snow distribution over the tundra area after a strong wind event, the volume of snow that moved during this event was estimated. By examining the spatial lagged autocorrelation (i.e. how far did the snow dunes move), the distance that the snow transported during this event could be derived. Furthermore, photographic and videographic records were obtained to document snow and ice conditions, and BROMEX field activities.

 ISBN: 978-1-61208-261-5

In an effort to trace the source and transport of bromide ions from the ice and snow reservoirs, two sea ice cores, 38 snow samples, and 20 blowing snow samples were collected at several locations in the vicinity of Barrow by Dartmouth College. The sea ice cores were each approximately 1.5 m long. Surface snow was collected at both sea ice core locations, at several locations in Elson Lagoon, at a tundra site, and along a 2-km East-West transect near the shoreline of the Chukchi Sea where samples were also collected for mercury analysis. Where possible, snow pits were dug to sample snow from different depths. Moreover, blowing snow samples were collected at four different heights (0.5 m, 1.5 m, 2.5 m, and 5.5 m) above the snow surface over a seven-day period. As a part of the ground-truthing efforts for the IceBridge aircraft measurement, surface temperature, surface height, snow depth, and ice thickness measurements were collected. In addition, in-situ measurements were taken to measure snow density and snow water equivalent.

The U.S. Naval Academy (USNA) also participated in BROMEX. CRREL and USNA personnel worked with members of the Barrow community to establish the opening of a 3 km of trail to the OOTI site and other locations in the Chukchi Sea. USNA successfully deployed IceGoat1 Buoy during BROMEX. This buoy reported near-real-time observations of air and sea temperatures, atmospheric pressure, position and images from two mounted webcams. Acoustic instrumentation systems were set up for under- and through-ice ambient noise and propagation loss measurements to characterize acoustic signatures of lead ruptures and closures. Sea ice, frost flowers, snow, brine icicle, and water samples were collected for chemical and biological analyses. Bulk snow and water samples were analyzed for ^{137}Cs and ^{134}Cs to look for the fingerprint of the 2011 Fukushima-Daiichi Nuclear Power Plant incident. Twenty bacterial cultures were made: 19 psychrophilic clones (obligate cold growth) isolated from ice core and seawater interface samples, and one psychrotolerant clone (in 4°C - 25°C) from a brine icicle sample. Also obtained was a small eukaryote to be studied for biofuels potential or for general characterization and potential toxicity.

V. SUMMARY

The BROMEX field campaign was successfully carried out across the sea, land, and air region around Barrow, Alaska. More than twenty institutions from U.S., Canada, U.K., and Germany participated in BROMEX. This is a major interdisciplinary science research to investigate impacts of Arctic sea ice reduction on atmospheric photochemical processes of bromine explosion, ozone and mercury depletion, and mercury deposition. Large datasets were obtained from the surface (sea ice and tundra snow), from aircraft (ALAR and NASA IceBridge P3), and from space (multiple international satellites). Valuable scientific findings have emerged from our initial analyses of BROMEX data, from which better measurement protocols and new research directions can be identified. While BROMEX helps improve our understanding of halogen processes in a changing Arctic, it has also initiated new science questions to be investigated in the future.

ACKNOWLEDGMENTS

The research carried out at the Jet Propulsion Laboratory, California Institute of Technology, and at NASA Goddard Space Flight Center was supported by the National Aeronautics and Space Administration (NASA) Cryospheric Sciences Program. Rigor is funded by NASA and the contributors to the International Arctic Buoy Programme (IABP), including the International Arctic Research Center, NASA, Naval Oceanographic Office (NAVO), NIC, NOAA, National Science Foundation (NSF), Office of Naval Research (ONR), and U.S. Coast Guard. The views, opinions, and findings contained in this report are those of the authors and should not be construed as an official National Oceanic and Atmospheric Administration, or any other U.S. government position, policy, or decision. We thank the Indian Space Research Organisation (ISRO) for Oceansat-2 satellite scatterometer data, Kelly Chance and Raid Suleiman of the Harvard-Smithsonian Center for Astrophysics for OMI observations in support of BROMEX, Jeff Schmaltz of NASA GSFC for setting up the BROMEX subsets from the LANCE MODIS Rapid Response system, the NIC team for BROMEX special support products, UMIAQ for field logistic assistance, the Barrow whaling community for mutual beneficial interactions, and Nok Acker of the Barrow Arctic Science Consortium for community outreach presentations and several radio broadcasts in Barrow. The tremendous success of the OOTI project was a result of the expertise of John Deary.

REFERENCES

[1] S. V. Nghiem, I. G. Rigor, D. K. Perovich, P. Clemente-Colón, J. W. Weatherly, and G. Neumann, "Rapid reduction of Arctic perennial sea ice," Geophys. Res. Lett., vol. 34, L19504, doi:10.1029/2007GL031138, Oct. 2007.

[2] S. V. Nghiem, I. G. Rigor, A. Richter, J. P. Burrows, P. B. Shepson, J. Bottenheim, D. G. Barber, A. Steffen, J. Latonas, F. Wang, G. Stern, P. Clemente-Colón, S. Martin, D. K. Hall, L. Kaleschke, P. Tackett, G. Neumann, and M. G. Asplin, "Field and satellite observations of the formation and distribution of Arctic atmospheric bromine above a rejuvenated sea ice cover," J. Geophys. Res., vol. 117, D00S05, doi:10.1029/2011JD016268, Mar. 2012.

[3] E. Kalnay et al., "The NCEP/NCAR 40-year reanalysis project," Bull. Am. Meteorol. Soc., vol. 77, pp. 437–471, doi:10.1175/1520-0477(1996) 077<0437:TNYRP>2.0.CO;2, 1996.

[4] R. de Beek, M. Weber, V. V. Rozanov, A. R. Ozanov, A. Richter, and J. P. Burrows, "Trace gas column retrieval and error assessment study for GOME-2, in Trace Constituents in the Troposphere and Lower Stratosphere," Adv. in Space Res., vol. 34, no. 4, pp. 727-733, 2004.

[5] P. Wennberg, "Atmospheric chemistry – Bromine explosion," Nature, vol. 397, pp. 299-301, 1999.

[6] W.-Y. Tsai, S. V. Nghiem, J. N. Huddleston, M. W. Spencer, B. W. Stiles, and R. D. West, "Polarimetric scatterometry: A promising technique for improving ocean surface wind measurements from space," IEEE Trans. Geosci. Remote Sens., vol. 38, pp. 1903-1921, Jul. 2000.

[7] SCAT-DP Team, Oceansat-2 Scatterometer algorithms for sigma-0, processing and products format, Vers. 1.1, 32 pp., Space Applications Centre, Ahmedabad, Gurajat, India, 2010.

[8] I. G. Rigor and J. M. Wallace, "Variations in the age of Arctic sea-ice and summer sea-ice extent," Geophys. Res. Lett., vol. 31, L09401, doi:10.1029/2004GL019492, 2004.

[9] http://www.chem.purdue.edu/shepson/alar.html (accessed Jan. 2013).

 ISBN: 978-1-61208-261-5

Specific Fatty Acid Status in the White Sea Herring From Different Bays of the White Sea in Regard to Ecological Factors

Role of Fatty Acids in Ecological and Biochemical Adaptations of Fishes in Sub-Arctic

Svetlana A. Murzina, Zinaida A. Nefedova, Nina N. Nemova, Pauli O. Ripatti
Environmental biochemistry lab
Institute of Biology of Karelian Research Centre of the Russian Academy of Sciences, IB KarRC RAS
Petrozavodsk, Russian Federation
e-mail: imagination@onego.ru

Svetlana N. Pekkoeva
Ecology and Biology Faculty
Petrozavodsk State University, PetrSU
Petrozavodsk, Russian Federation
e-mail: pek-svetlana@mail.ru

***Abstract*—Fatty acid status of the White Sea herring from Dvina, Kandalaksha and Onega Bays of the White Sea in autumn was investigated. The fatty acid profile of the herring groups from studied sites was characterized by high amount of monounsaturated fatty acids, among which 18:1(n-9) and 16:1(n-7) dominated. The herring from Kandalaksha Bay had higher ($p \leq 0.05$) level of 18:1(n-9) fatty acid than the fish from Onega Bay, whereas the last one was characterized by low ($p \leq 0.05$) level of 16:1(n-7). Polyunsaturated fatty acids (PUFA) were the second largest group in the herrings, mainly because of (n-3) fatty acids. In the herring from Onega Bay, the level of 22:6(n-3) was significantly ($p \leq 0.05$) higher than in other fishes. Besides that, this fishes were characterized by high level of (n-3)/(n-6) PUFA, 18:3(n-3)/18:3(n-6) and 16:0/18:1(n-9) ratios. Detected lipid status reflects ecological and biochemical features of fish adaptation in relation to specific ecological factors of the inhabitation areas of the White Sea and choice of optimal and adequate survival strategy in sub-Arctic. The results of this work present information about some features of mechanisms of adaptations on the level of lipid spectra and the role of fatty acid constituents in ecological and biochemical adaptions of the White Sea herring.**

Keywords-biochemical adaptation; fatty acids; lipids; the White Sea herring; Sub-Arctic

I. INTRODUCTION

Lipids and fatty acids have important functions in cell metabolism and play a significant role in biochemical adaptations of organisms to changing environmental conditions (abiotic, biotic, anthropogenic factors) [1-4]. Fish lipids, mainly their fatty acids (FA), are the basic source of metabolic energy and structural elements for their growth, development, reproduction, and survival [1-3]. Especially, it concerns fishes that have high level of lipids in their bodies as herring, salmon, trout etc. [5-8]. Fatty acids are one of the most sensitive lipid components that take active part in compensatory mechanisms of adaptation of organisms in normal and in stress [1-2]. Quick change of lipid and fatty-acid profile of fish tissues and organs contributes to optimal process of life activity and their adaptation, including thermal adaptation, to changing environment [3].

The population of the White Sea herring *Clupea pallasii marisalbi* Berg (Clupeiformes, Clupeidae) is one of the similar forms of Pacific herring and one of the main and the most commercial fish in the White Sea. The local groups of herring are subject to particular hydrological conditions in different bays of the sea [9]. The biochemical studies of the White Sea herring are not numerous. Biochemical adaptations to specific ecological conditions of the White Sea (specific temperature regime, high speed of currents, water exchange with the Barents Sea, small depths, low concentration of mineral substances and organic compounds, low level of salinity, relatively short vegetation period, etc.) cannot ignore changes in lipid status of the fish.

Fatty acid status of the White Sea herring from different bays (Dvina, Kandalaksha and Onega bays) in autumn season was investigated.

The results of this research will contribute to the current knowledge about the role and functions of lipids that take part in development and formation of biochemical adaptations of other fish species. They also present new information about the features of mechanisms of adaptations on the level of lipid status of the studied fish in the sub-Arctic region.

The presented paper consists of next sections: material and methods, results of fatty acid analysis of the White Sea herring from different Bays, discussion, conclusion and acknowledgement.

II. MATERIAL AND METHODS

The White Sea herring adults were collected in October, 2010 in Dvina ($64^{o}57'$ $38^{o}23'$), Kandalaksha ($67^{o}02'$ $32^{o}23'$) and Onega Bays ($64^{o}59'$ $36^{o}37'$) of the White Sea at depth 50, 25 and 38 meters and at temperature 6.5^{o}, 2.9^{o} and 6.7^{o}C, respectively, according the method described by [10]. In total 66 individual specimens (n) were analyzed.

Flesh of the fish was homogenized in 10 volumes (10 ml each) of 96% ethyl alcohol mixed with 0.001% of the antioxidant. Sample homogenates were placed in glass vials and stored onboard the ship in a cold room until delivery to the laboratory. The material was then fixed in a solvent system of chloroform:methanol (2:1, volume/volume), and

 ISBN: 978-1-61208-261-5

total lipids (TL) were extracted following the method [11]. The residues recovered after lipid extraction of the flesh were dried over phosphoric anhydride until the samples had reached a constant weight. The residues were weighted to determine the approximate percentage of total lipids (T) on a dry-weight basis (1), where β – lipids extracted (g) and α – residue weight (g):

$$T = \beta * 100/(\alpha + \beta). \quad (1)$$

The fatty acids composition of the total lipids was analyzed by gas-liquid chromatography. Fatty acid methyl esters (FAME) were identified with a "Chromatek-Crystall-5000.1" (Russia) gas chromatograph with flame-ionization detector on a Zebron Capillary Gas Chromatographic Column (Phenomenex, USA). The isothermic column regime was used (225^0C), temperature of detector – 250^0C; temperature of evaporator – 240^0C. For recording and integration "Chromatek-Analytik-5000.1" software (Russia) was applied.

The research was carried out using the facilities of the Equipment Sharing Centre of the Institute of Biology, KarRC of RAS

Data were tested for normal distribution. Differences between means of fatty acids of total lipids in herrings from studied areas of the sea were analyzed by analysis of variance ANOVA ($p \leq 0.05$).

III. RESULTS

The biochemical analysis showed that the herring from Kandalaksha Bay had higher level of TL (41.7% dw) compared to the herring from Dvinsky and Onega Bays (34.5%; 31.8% dw, respectively) (Table I). In Table 1, Values in the same row with the same superscripted letter are not significantly different ($p>0.05$) among fishes from different areas of the Sea and values in the same row with the different superscripted letter are significantly different ($p \leq 0.05$) among fishes.

TABLE I. TOTAL LIPIDS (% DRY WEIGHT) AND FATTY ACID SPECTRUM (% OF TOTAL FA) IN THE WHITE SEA HERRING FROM DVINA, KANDALAKSHA AND ONEGA BAYS IN AUTUMN. DATA ARE M±M.

FA/Bay	Dvina (A)	Kandalaksha (B)	Onega (C)
n	20	21	25
TL	34.5±0.6 ^{BC}	41.7±1.4 ^{AC}	31.8±0.8 ^{AB}
12:0	0.30±0.21 ^{B}	0.04±0.01 ^{AC}	0.18±0.01 ^{B}
14:0	10.53±0.35 ^{BC}	12.40±0.28 ^{AC}	8.80±0.43 ^{AB}
15:0	0.89±0.03 ^{BC}	0.57±0.02 ^{AC}	0.72±0.03 ^{AB}
16:0	21.66±0.47	21.40±0.35	22.26±0.62
17:0	0.47±0.06 ^{C}	0.37±0.06 ^{C}	0.90±0.02 ^{AB}
18:0	2.25±0.06 ^{BC}	1.66±0.07 ^{AC}	3.21±0.17 ^{AB}
20:0	0.87±0.03 ^{B}	0.66±0.05 ^{AC}	0.94±0.05 ^{B}
24:0	0.16±0.01 ^{BC}	0.12±0.01 ^{AC}	0.25±0.02 ^{AB}
Sum SFA	37.12±0.80	37.23±0.66	37.26±0.81
14:1(n-5)	0.39±0.01 ^{C}	0.37±0.01 ^{C}	0.34±0.01 ^{AB}
16:1(n-9)	0.73±0.06	0.40±0.04 ^{C}	0.74±0.10 ^{B}
16:1(n-7)	11.31±0.29 ^{C}	11.45±0.22 ^{C}	7.73±0.24 ^{AB}
16:1(n-5)	0.25±0.02	0.25±0.02	0.29±0.03
17:1(n-7)	0.35±0.04 ^{C}	0.34±0.04 ^{C}	0.59±0.03 ^{AB}
18:1(n-9)	19.80±0.35	20.14±0.33 ^{C}	18.40±0.73 ^{B}
18:1(n-7)	4.05±0.28 ^{BC}	3.19±0.26 ^{A}	3.39±0.10 ^{A}
18:1(n-5)	0.82±0.05 ^{BC}	1.09±0.05 ^{AC}	0.69±0.03 ^{AB}
20:1(n-11)	0.24±0.05	0.17±0.02	0.58±0.24
20:1(n-9)	1.46±0.12 ^{B}	2.10±0.21 ^{A}	1.93±0.56
20:1(n-7)	0.35±0.01	0.33±0.01	0.33±0.02
22:1(n-11)	0.88±0.08 ^{B}	1.44±0.17 ^{A}	1.40±0.46
22:1(n-9)	0.32±0.02	0.32±0.02	0.79±0.42
22:1(n-7)	0.23±0.01 ^{C}	0.21±0.01 ^{C}	0.43±0.03 ^{AB}
24:1(n-9)	0.22±0.08 ^{C}	0.27±0.08 ^{C}	1.18±0.04 ^{AB}
Sum MUFA	41.40±0.75	42.06±0.51	38.81±1.57
16:2(n-9)	0.23±0.02 ^{BC}	0.16±0.02 ^{A}	0.13±0.02 ^{A}
18:2(n-9)	0.08±0.01	0.06±0.01	0.06±0.01
20:2(n-9)	0.09±0.01	0.10±0.01 ^{C}	0.07±0.01 ^{B}
22:2(n-9)	0.05±0.01 ^{C}	0.05±0.01 ^{C}	0.02±0.01 ^{AB}
Sum (n-9) PUFA	0.44±0.04 ^{C}	0.37±0.02 ^{C}	0.29±0.02 ^{AB}
16:2(n-7)	0.17±0.02 ^{BC}	0.09±0.01 ^{A}	0.10±0.02 ^{A}
18:2(n-7)	0.05±0.01 ^{C}	0.07±0.01 ^{C}	0.31±0.07 ^{AB}
Sum (n-7) PUFA	0.22±0.02	0.16±0.02 ^{C}	0.41±0.09 ^{B}
16:2(n-6)	0.41±0.05 ^{BC}	0.20±0.03 ^{A}	0.20±0.02 ^{A}
16:3(n-6)	0.35±0.03 ^{BC}	0.21±0.03 ^{AC}	0.01±0.00 ^{AB}
18:2(n-6)	1.31±0.05 ^{C}	1.21±0.02 ^{C}	1.06±0.05 ^{AB}
18:3(n-6)	0.15±0.01 ^{B}	0.11±0.01 ^{AC}	0.15±0.01 ^{B}
20:2(n-6)	0.22±0.01 ^{B}	0.20±0.01 ^{AC}	0.24±0.01 ^{B}
20:4(n-6)	0.28±0.02	0.30±0.01	0.29±0.02
Sum (n-6) PUFA	3.52±0.16 ^{BC}	2.70±0.07 ^{A}	2.58±0.09 ^{A}
18:3(n-3)	0.76±0.06 ^{B}	0.92±0.03 ^{A}	0.93±0.07
18:4(n-3)	1.33±0.10 ^{BC}	1.75±0.07 ^{A}	2.12±0.16 ^{A}
20:4(n-3)	0.42±0.04 ^{BC}	0.66±0.03 ^{AC}	0.53±0.03 ^{AB}
20:5(n-3)	6.51±0.52	6.61±0.31	7.38±0.47
22:6(n-3)	5.25±0.45 ^{C}	5.11±0.27 ^{C}	7.01±0.65 ^{AB}
Sum (n-3) PUFA	15.12±1.15 ^{C}	15.84±0.68 ^{C}	19.19±1.35 ^{AB}
Sum PUFA	21.48±1.38	20.71±0.74	23.92±1.48
(n-6)/(n-3)	0.26±0.02 ^{BC}	0.18±0.01 ^{AC}	0.15±0.01 ^{AB}

 ISBN: 978-1-61208-261-5

18:3(n-3)/18:2(n-6)	0.58±0.04 ^{BC}	0.76±0.02 ^{AC}	0.89±0.05 ^{AB}
16:0/18:1(n-9)	1.10±0.31 ^{C}	1.07±0.27 ^{C}	1.24±0.05 ^{AB}

The fatty acid spectrum of total lipids of the White Sea herring from all investigated bays were performed by monounsaturated fatty acids (MUFA) (from 38.81 to 42.06% of total FA), among which 18:1(n-9) and 16:1(n-7) FA dominated (within the limits 18.40 – 20.14% and 7.73 – 11.45% of total FA, respectively) (Table 1). The herring from Kandalaksha Bay had higher ($p \leq 0.05$) level of 18:1(n-9) FA than the fish from Onega Bay, whereas the last one was characterized by low ($p \leq 0.05$) level of 16:1(n-7) FA. It was determined that the amount of other MUFAs – 18:1(n-7), 20:1(n-9), 22:1(n-11), 22:1(n-7), 24:1(n-9) – did not exceed 5.0 % of total FA but their levels were significantly different ($p \leq 0.05$) among fishes from different bays of the sea.

It was shown that the level of saturated FA (SFA) was high. Among SFA – 16:0 and 14:0 FA dominated and ranged from 21.40 to 22.26% and from 8.80 to 12.40% of total FA, respectively in all investigated groups of herring. Low concentration of 18:0 FA (1.66 – 3.21% of total FA) was detected in relation to fish from all sea regions.

Polyunsaturated FA (PUFA) amount was within the limits from 20.71 to 23.92% of total FA, mainly because of (n-3) polyenic FA (15.12 – 19.19% of total FA) in the White Sea herring from all investigated areas. Among (n-3) PUFA – 20:5(n-3) and 22:6(n-3) were dominated. The White Sea herring from Onega Bay was slightly distinguished by high level ($p \leq 0.05$) of these acids (mainly 22:6(n-3)) and (n-3)/(n-6), 18:3(n-3)/18:2(n-6) and 16:0/18:1(n-9) ratios.

Thus, high level of total MUFAs ($p \geq 0.05$) was typical for the White Sea herring from all the studied inhabitations of the White Sea. The variations of some FA: with high level 17:0, 17:1(n-7), 18:0, 18:2(n-7), 22:1(n-7), 24:1(n-9), 22:6(n-3) and low level - 14:0, 16:1(n-7), 16:3(n-6), 18:1(n-5), 18:2(n-6), - differed the herring from Onega bay from others. Besides that, this fishes were characterized by high level of (n-3)/(n-6)PUFA, 18:3(n-3)/18:3(n-6) and 16:0/18:1(n-9) ratios.

IV. DISCUSSION

Fatty acid status of the White Sea herring from different bays of the White Sea (Dvina, Kandalaksha and Onega Bays) in autumn season was investigated. High level of MUFAs is one of the typical features of aquatic marine organisms in northern latitudes. MUFA were the dominant FA group in all the herring groups in studied sites of the White Sea. Among MUFA – 18:1(n-9) and 16:1(n-7) were the most abundant. It is known that some MUFAs are dietary derived and they are trophic biomarkers for marine organisms: 18:1(n-9) FA is the main biomarker of dinoflagellates and bacterial plankton while 16:1(n-7) FA is the biomarker of diatoms microalgae [12-16]. Dinoflagellates and diatoms microalgae make the main contribution to biomass of the White Sea phytoplankton [17]. In the end of October (time of material collection) the phytoplankton bloom period finishes. In water there are just mass species of flagellates and diatoms algae disappears [18]. This fact explains lower level of 16:1(n-7) FA in herring from Onega Bay in comparison with fish from other places of the White Sea.

It was outlined that herrings of the studied bays had low level of 20:1(n-9) and 22:1(n-11) FA (1.46 – 2.10 % and 0.88 – 1.44 % of total FA, respectively) that are synthesized *de novo* only by planktivorous species *Calanus* spp. [15] [19]. Therefore, in this period these zooplankton species made up small amount of herring diet that was evidently reflected on FA spectrum of the White Sea herring.

Respectively high level of SFA, the domination of 16:0 and 14:0 FA, was connected not only with *de novo* synthesis but also with their accumulation related to feeding on phyto- and zooplankton, presence and availability of which differed in food web and food habits of herring from different areas of the White Sea. Low level of 14:0 as well as 16:1(n-7) FA, biomarkers of diatoms, in herrings from Onega Bay in comparison with herrings from other studied area might be connected with decrease of producing capacity of diatoms algae in this period. The 16:0/18:1(n-9) ratio was higher in herring from Onega Bay. It indicated higher degree of intensity of lipid metabolism [20].

Low level of PUFA, especially 22:6(n-3) FA among the White Sea herring in comparison with other arctic and subarctic fish species shows that these FA played secondary role in terms of biomembrane functioning in these conditions. The correlation between (n-3) and (n-6) PUFA plays a specific role in organism due to competitive relations in the process of their metabolism [21]. It is also shown that cold water pelagic fishes have higher (n-3) PUFA level that satisfy their need in essential fatty acids more than (n-6) and (n-9) PUFA [4] [22] [23]. The (n-3)/(n-6) PUFA ratio was higher in herring from Onega Bay than among fish groups in other bays of the sea. The change of lipid unsaturation degree is one of the basic mechanisms of regulation of activity of membrane connected enzymes under environment fluctuations [1] [24].

V. CONCLUSION

The difference in terms total lipids and fatty acids among the White Sea herring from the studied bays of the White Sea was presented. The results of the paper present information about some features of mechanisms of adaptions on the level of lipid spectra and the role of fatty acid constituents in ecological and biochemical adaptations of fishes under study. It showed various influence of the complex of ecological factors, in this research mainly biotic (trophic). The determined spectra of fatty acids among the White Sea herring from its different bays confirm that in the period of fattening the main source of their nutrition were the diatoms algae and dinoflagellates and the income of copepods was small. Such lipid status reflects ecological and biochemical features of fish adaptation in relation to specific hydrobiological and trophoecological factors of the inhabitation areas of the White Sea and choice of optimal and adequate survival strategy in future. Detailed analysis of

 ISBN: 978-1-61208-261-5

separate fatty acids, their ratios of herrings from different sites of the White Sea in respect to abiotic factors (temperature, depth, water currents) will be given in future. The results of this work will contribute to the current knowledge about the role and functions of lipids and lipid components in biochemical adaptations of fishes from high latitudes.

ACKNOWLEDGMENT

The research was supported by The President of the Russian Federation Grants NSh-1642.2012.4 and MK-666.2011.4; RFBR 11-04-00167-a; The Presidium of RAS Program of Fundamental Research "The Living nature: contemporary condition and problems of development" project "Inventory of aquatic organisms communities in Arctic and sub-Arctic ecosystems in changing biotic and abiotic factors"; FCP "Mechanisms of adaptation and sustainability of organisms and populations of plants and animals in the North (physiological, biochemical and molecular-genetic aspects)".

REFERENCES

[1] E.M. Kreps, Lipids of cell membrane. Evolution of brain lipids. Adaptations function of lipids.

[2] V.S. Sidorov, Ecological biochemistry of fishes.

[3] P.W. Hochachka and G.N. Somero, Biochemical adaptation: mechanism and process in physiological evolution.

[4] M.T. Arts and C.C. Kohler, "Health and conditions in fish: the influence of lipids on membrane competency and immune response," in Lipids in aquatic ecosystems, M.T. Arts, M.T. Brett, M.J. Kainz, Eds. Dordrecht, Heidelberg, London, New York: Springer, 2009, pp. 237-257.

[5] R.J. Henderson and S. Almatar, "Seasonal changes in the lipid composition of herring *Clupea harengus* in relation to gonad maturation," Journal of the Marine biological Association of the U.K., 1989, № 69, pp. 323–334. doi: 10.1017/s0025315400029441.

[6] D.R. Tocher, "Metabolism and functions of lipids and fatty acids in Teleost fish," Reviews in Fisheries Science, vol. 12, 2003. pp. 107-182.

[7] S.A. Murzina, Z.A. Nefedova, P.O. Ripatti, N.N. Nemova, and L.V. Markova, "Dynamics of fatty acid composition of total lipids during embryonic development of Atlantic Salmon *Salmo salar* L.," Russian journal of Developmental biology, vol.43, 2012, pp. 131-136, doi: 10.1134/S1062360412020051.

[8] D.S. Pavlov, N.N. Nemova, E.A. Kirillova, P.I. Kirillov, Z.A., Nefedova, and S.A. Murzina, "Lipid content in the young-of-the-year sockeye salmon *Oncorhynchus nerka* during feeding migration (the Ozernaya River, Western Kamchatka)," Doklady biological sciences, vol. 445, 2012, pp. 232-238, doi: 10.1134/S0012496612040023.

[9] V.V. Kuznetsov, The White Sea and its biological features of flora and fauna. Moscow: Publishing house AS USSR, 1960, pp. 57-298.

[10] A.V. Semushin, V.S. Sherstkov, and V.A. Rukhlova, "Diversity of fish species in the trawl catches in the southeastern Barents Sea in 1980–2008", Journal of ichthyology, vol. 51, 2011, pp. 717-737, doi: 10.1134/S0032945211050201.

[11] J. Folch, M. Lees, and G.H. Sloane Stanley, "A simple method for the isolation and purification of total lipids from animal tissue", Journal of biological chemistry, vol. 226, 1957, pp. 497-509.

[12] A.C. Viso and J.C. Marty, "Fatty acids from 28 marine microalgae," Phytochemistry, vol. 34, 1993, pp. 1521-1533. doi: 10.1016/S0031-9422(00)90839-2.

[13] C. Viron, A. Saunois, P. Andre, B. Perly, and M. Laffose, "Isolation and identification of unsaturated fatty acid methyl esters from marine micro-algae," Analytica Chimica Acta, vol. 409, 2000, pp. 257-266, doi: 10.1016/S0003-2670(99)00857-0.

[14] H. Auel, M. Harjes, R. da Rocha, D. Stubing, and W. Hagen, "Lipid biomarkers indicate different ecological niches and trophic relationships of the Arctic hyperiid amphipods *Themisto abyssorum* and *T. libellula*," Polar biology, vol. 25, 2002, pp. 374-383, doi: 10.1007/s00300-001-0354-7.

[15] M. Graeve, M. Lundberg, M. Boer, G. Kattner, H. Hop, and S. Falk-Petersen, "The fate of dietary lipids in the Arctic ctenophore *Mertensia ovum* (Fabricius 1780)," Marine biology, № 153, pp. 643-651, doi: 10.1007/s00227-007-0837-3.

[16] J. Legezynska, M. Kedra, and W. Walkusz, "When season does not matter: summer and winter trophic ecology of Arctic amphipods," Hydrobiologia, vol. 684, 2012, pp. 189-214, doi: 10.1007/s10750-011-0982-z.

[17] L.B. Iljash and L.S. Zitina, V.D. Fedorov, Phytoplankton of the White Sea. Moscow: Janus-K, 2003, pp. 48-154.

[18] V.Ja. Berger, Production potential of the White Sea. St. Petersburg: ZIN RAS, 2007, pp. 66-131.

[19] S. Falk-Petersen, C.C.E. Hopkins, and J.R. Sargent, "Trophic relationships in the pelagic, arctic food web," Proc. 24th Europ. Mar. Biol. Symp., 1990, pp. 315-333.

[20] E.I. Kal'chenko, T.L. Videnskaya, and M.I. Yur'eva, "Feeding and fatty acid content of wild and captured juveniles of dog-salmon during keeping in river fishponds," Proc. International conference Modern problems of physiology and biochemistry of aquatic organisms, KarRC RAS, 2004, pp. 58.

[21] M.G. Sergeeva and A.T. Varfolomeeva. The cascade of arachidonic acid. Moscow, Narodnoe obrazovanie, 2006, pp. 21-38.

[22] J.R. Cejas, E. Almansa, S. Jerez, A. Bolanos, B. Felipe, and A. Lorenzo, "Changes in lipid class and fatty acid composition during development in white seabream (*Diplodus sargus*) eggs and larvae", Comparative biochemistry and physiology B, № 2, 2004, pp. 209-216, doi: 10.1016/j.cbpc.2004.07.010.

[23] S.J. Iverson, "Tracing aquatic food webs using fatty acids: from qualitative indicators to quantitative determination," in Lipids in aquatic ecosystems, M.T. Arts, M.T. Brett, M.J. Kainz, Eds. Dordrecht, Heidelberg, London, New York: Springer, 2009, pp. 281-309.

[24] A.A. Boldyrev, E.I. Kaivarainen, and V.A. Ilykha, Biomembranology. KarRC RAS, Petrozavodsk, 2006, pp. 24-102.

 ISBN: 978-1-61208-261-5

Monitoring of Residential Air Quality by Formaldehyde Biochemical Gas Sensor for Indoor Public Health

High sensitive (sub-ppb) bio-sniffer for residential VOC assessment

Toshifumi Yamashita, Kumiko Miyajima, Takahiro Arakawa, Hiroyuki Kudo, Kohji Mitsubayashi
Institute of Biomaterials and Bioengineering,
Tokyo Medical and Dental University, Tokyo, Japan
ty.bdi@tmd.ac.jp, ku.bdi@tmd.ac.jp, ta.bdi@tmmd.ac.jp,
hk.bdi@tmd.ac.jp, m.bdi@tmd.ac.jp

Tomoko Gessei
Tokyo Metropolitan Industrial Technology Research Institute, Tokyo, Japan
ge.bdi@tmd.ac.jp

***Abstract*— An optical fiber biochemical gas sensor (bio-sniffer) for assessment of indoor formaldehyde was fabricated and tested. The bio-sniffer measures formaldehyde vapor as fluorescence of reduced nicotinamide adenine dinucleotide (NADH), which is the product of formaldehyde dehydrogenase (FALDH) reaction. Usually, an enzyme loses its specific activity in the gas phase. This makes biochemical gas monitoring difficult. We used a micro flow-cell with a FALDH immobilized membrane to prevent the FALDH from deactivation. An ultraviolet light emitting diode (UV-LED) with peak emission of 335nm was employed as an excitation light source. Emission of the UV-LED was introduced to the optode through an optical fiber and fluorescence of NADH was picked up coaxially at the optode. In order to improve the sensitivity, a photomultiplier tube was utilized as a photodetector. Consequently, continuous FA monitoring with biochemical method was successfully conducted with high sensitivity and high selectivity. A real-sample test was also carried out with the bio-sniffer. According to the results, it is expected to be useful in fast and convenient monitoring of indoor FA.**

Keywords- residential formaldehyde; bio-sniffer; volatile organic compound; public health.

I. INTRODUCTION

Formaldehyde (FA) is a reactive and flammable aldehyde which is well known as one of the harmful volatile organic compounds (VOCs). Although FA is also produced in natural processes [1], it is mainly emitted to the living environment by human activities. One of the main emission sources of indoor FA is urea-formaldehyde resins in pressed wood products, such as particleboard and fiberboard used in cabinetry and furniture. A combination of respiratory disease, allergic dermatitis and other ailments so called sick building syndrome (SBS), is associated with chronic exposure to FA [2-3]. Therefore, indoor FA levels are occasionally utilized to assess indoor air qualities. The guideline for indoor FA is determined to 80 ppb from its acute toxicity by world health organization (WHO). Although the WHO standard is held in many countries, there are still serious health problems caused by chronic exposure to FA even less than 80 ppb.

The relationship between the indoor FA levels and related health damages are usually investigated using chromatographic methods [4]. However, these methods are too time-consuming to monitor the daily fluctuation of indoor FA levels. Hence, solid-state gas sensors with gas-sensitive oxides are expected in monitoring of indoor VOCs for their stability, reduced cost and fast response [5-10]. Considering the monitoring of indoor FA, it is also important to enhance the selectivity to other chemicals since the measurement is conducted under the presence of many chemicals. Improving the selectivity of real-time gas monitoring in mind, we previously reported a biochemical gas sensor (bio-sniffer) that utilizes enzyme to recognize the target substance [11].

In this work, we have constructed a fiber-optic biochemical gas sensor for continuous monitoring of indoor formaldehyde with high sensitivity and tested by monitoring fluctuation of FA levels using real-sample. We report the design, structure, characteristics and latest result of indoor FA monitoring.

II. EXPERIMENTAL

A. Design and Fabrication

The bio-sniffer measures FA as fluorescence of nicotinamide adenine dinucleotide (NADH), which is the product of formaldehyde dehydrogenase (FALDH) reaction given as following equation.

$$FA + NAD^+ + H_2O \xrightarrow{FALDH} \text{formic acid} + NADH + H^+ \quad (1)$$

The bio-sniffer consists of an UV-LED-based excitation system, a photomultiplier tube (PMT) and an optical fiber probe with a flow-cell. The UV-LED based excitation system was constructed by attaching an UV-LED (UVTOP® BL335, Sensor Electronic Technology, Inc., USA) on a custom-fabricated UV-LED power supply (KLV CO., LTD., Japan) with an adjustable SMA connector.

 ISBN: 978-1-61208-261-5

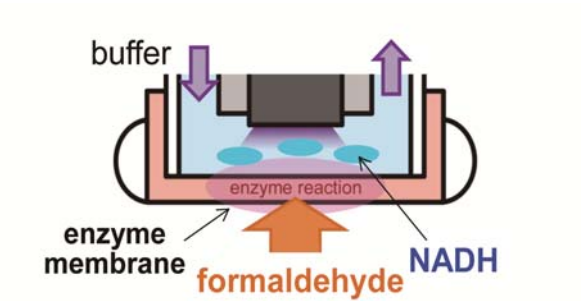

Figure 1. Principle of the fiber-optic bio-sniffer for FA vapor.

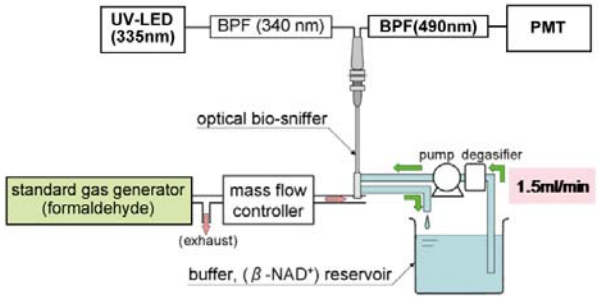

Figure 2. Experimental set-up for characterization of the bio-sniffer.

The excitation system and the PMT (C9692, Hamamatsu Photonics, Co., Ltd, Japan) were connected to an optical fiber probe (F1000-900, core diameter: 1.0 mm, Ocean Optics Inc., USA) using an optical fiber assembly (BIF600-UV/VIS, Ocean Optics Inc., USA). The excitation light and the fluorescent light were filtered using a band-pass filter (BPF: 490-510 nm) and a long-pass filter (LPF: >400 nm) purchased from Asahi Spectra Co. LTD. (Japan), respectively. A flow cell, on which an enzyme immobilized membrane, was attached at the end of the optical fiber probe. The enzyme membrane was prepared as follows: FALDH (FALDH, EC 1.2.1.1, 1 units/mg, solid, from Pseudomonas sp., Funakoshi Co., Ltd., Tokyo, Japan) with an activity of 1 unit mg^{-1} of protein was first immobilized onto a hydrophilic PTFE (H-PTFE) membrane filter (Porosity: 80 %, Pore size: 0.2 µm, JGWP14225, Millipore Co., USA) by curing a mixture of 2-methacryloyloxyethyl phosphorylcholine (MPC) copolymerized with 2-ethylhexyl methacrylate (EHMA) solution (1µl cm^{-2}) and FALDH (50 units cm^{-2}) on the H-PTFE membrane filter (4 °C, 180 min).

Figure 1 represents the working principle of the bio-sniffer. Since the enzyme is immobilized at the hydrous sensing membrane, the FA vapor at the neighborhood of the probe is easily dissolved into the flow-cell. As explained in eq (1), FALDH produces formic acid and NADH under the presence of FA and NAD^+. Fluorescence of the NADH is coaxially introduced into the optical fiber probe and measured with the PMT. Phosphate buffer which contained NAD^+ is continuously circulated in the flow-cell to prevent enzyme from deactivation, to remove the products of enzyme reaction and to rinse the excessive substrate. The NADH produced at the sensing region is immediately removed from the sensing region. Therefore, the output of the fiber-optic bio-sniffer is determined by the trade-off of the FA level and the removal rate of NADH (i.e. flow-rate of the phosphate buffer). This indicates that the sensing region of the bio-sniffer is always refreshed by the circulation of the phosphate buffer which contained NAD^+.

B. *Characterization of the FA bio-sniffer*

Characterization of the bio-sniffer was carried out using a standard gas generator (Permeater, Type: PD-1B, Gastec Corp., Kanagawa, Japan) [12]. Figure 2 shows the experimental set-up for characterization of the fiber-optic bio-sniffer. The UV-LED was operated with a constant forward current of 20 mA for excitation of NADH. The excitation light was coupled into the optical fiber and guided to the probe. During the measurement, phosphate buffer (pH 8.0, 80 mM) with NAD^+ (20 mM) was circulated into the flow-cell (flow rate: 1.5 ml/min). Various concentrations of standard FA vapor were supplied with the standard gas generator. The flow-rate of the sample gas was fixed at 200 ml/min. Fluorescent signal was measured with the PMT and the signal was recorded using a laptop PC.

In order to confirm the usefulness of our system for real indoor airs, fluctuation of the FA levels induced by a real-indoor air was also investigated using the bio-sniffer in real-time.

III. RESULTS AND DISCUSSION

A. *Spectral response to FA vapor*

First of all, spectral response to formaldehyde vapor was investigated. Fluorescent spectrum of NADH was measured by replacing the PMT with a fiber-optic spectrometer. A cut on wavelength of 400nm was employed instead of the BPF (490nm). Figure 3 shows the spectral responses of the bio-sniffer. The line labeled 0 ppm represents the initial response and 5.0 ppm is the spectral response to 5.0 ppm FA vapor. In both cases, phosphate buffer which contained NAD^+ was circulated. Fluorescence increased as the concentration of the gaseous FA increased. The peak wavelength of the spectrum was 491nm, which is consistent with our previous reports [11]. The result indicates that NADH was successfully produced by enzyme reaction of FALDH (eq.1).

 ISBN: 978-1-61208-261-5

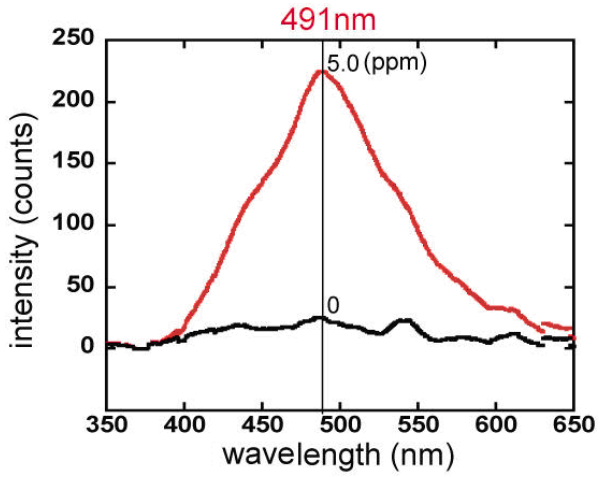

Figure 3. Spectral response of the bio-sniffer.

B. *Characteristics of the bio-sniffer for FA vapor*

After the spectral investigation, characterization of the bio-sniffer was carried out using the PMT as a photodetector and the BPF (490 nm). At first, the dynamic response to the FA exposure was investigated. Figure 4 shows the change of fluorescent response to FA. Exposure to Standard FA was conducted from 2 to 10 min. Only the carrier gas, which impurities were removed with activated carbon filter, was flown into the sensing region before and after the measurement.

At the beginning of FA exposure, the fluorescent signal increased immediately and became stable in approximately 90 seconds. And the signal decreased down to the initial value after the switching into carrier gas. The increase of the signal can be associated with the production of NADH as mentioned above, and the decrease of the signal is the resulted by the circulation of phosphate buffer. Considering the working mechanism, the fluorescent signal can be increased by reducing the flow-rate of the buffer circulation. The lower detection limit was 2.5 ppb, with the simple single LED excitation system. This can be improved by increasing the intensity of the excitation light by using multiplied LED system. The selectivity of the bio-sniffer was also investigated. Acetaldehyde, acetone, benzene, methanol and ethanol (5.0 ppm) was also tested using the bio-sniffer with FALDH. The maximum fluorescence was 1.3% of FA in case of acetaldehyde and no significant crosstalk was found in case of other chemicals.

In order to confirm the possibility of indoor FA monitoring, we also conducted a real-sample test. First the pure carrier gas was applied and confirmed the initial level. After that, air in the laboratory was applied to the sensing region. As a result, the fluorescence increased immediately and the FA level was estimated to 20 ppb at that time while it varies by the temperature or position in the room.

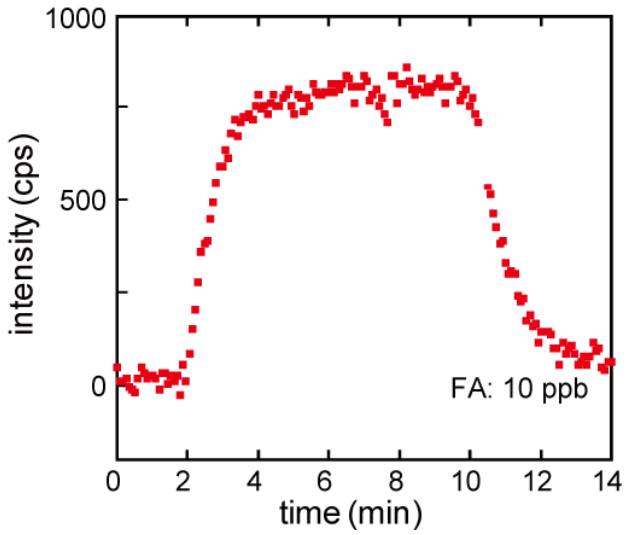

Figure 4. Typical change of the fluorescece during FA exposure. Standard FA vapor (10.0 ppb) was applied to the sensing region from 2 min to 10 min.

IV. CONCLUSIONS

A bio-sniffer for FA vapor was fabricated and confirmed to be useful for indoor FA monitoring. Since the bio-sniffer uses an enzyme for molecular recognition, high selectivity was achieved. The optical measurement system also reduces the effect of interferences in comparison with electrochemical methods. High sensitive detection system with the PMT provided high sensitivity to FA vapor. Using the optimized multi-LED system, it is expected to be able to monitor sub-ppb level FA in real-time.

ACKNOWLEDGMENT

This work was partly supported by Japan Society for the promotion of Science (JSPS) Grant-in-Aid for Scientific Research System, Japan Science and Technology Agency (JST) and MEXT (Ministry of Education, Culture, Sports, Science and Technology) Special Funds for Education and Research “Advanced Reasearch Program in Neo-Biology”.

REFERENCES

[1] R. Guicherit and F.L. Schulting, “The occunence of organic chemicals in the atmosphere of the Netherland,” Sci Total Environ. 43, 1985, pp. 193–219.

[2] J. Gamble, “Effects of formaldehyde on the respiratory system.” In: Gibson JE, ed. Formaldehyde toxicity. Hemisphere & McGraw Hill, Washington DC, 1983, pp. 175-197.

[3] H. Maibach, “Formaldehyde: Effects on animal and human skin.” In: Gibson JE, ed. Formaldehyde toxicity. Hemisphere & McGraw Hill, Washington DC, 1983, pp. 166-174.

[4] J. Levin, K. Andersson, R. Linndahl, and C. Nilsson, “Determination of sub-parts-per-million levels of formaldehyde in air using active and passive sampling on 2,4

 ISBN: 978-1-61208-261-5

dinitrophenylhydrazine-coated glass fibre and high-performance liquid chromatography," Anal. Chem. 57, 1985, pp. 1032–1035.

[5] J.A. Dirksen, K. Duval, and T.A. Ring. "NiO thin-film formaldehyde gas sensor," Sens. Actuator-B 80, 2001, pp. 106–115.

[6] T. Seiyama, A. Kato, K. Fujiishi, and M. Nagatani, "A new detector for gaseous components using semiconductive thin films," Anal. Chem. 34, 1962, pp. 502–1506.

[7] M. Tonoike, "Current status and future view of development for odorantsensors," Bull. Electrotechn. Lab. 52, 1988, pp. 63–79.

[8] Y. Hiranaka, T. Abe, and H. Murata, "Gas-dependent response in the temperature transient of SnO2 gas sensors," Sens. Actuators-B 9, 1992, pp. 177-182.

[9] T. Maekawa, J. Tamaki, N. Miura, and N. Yamazoe, "Development of SnO2-based ethanol gas sensor," Sens. Actuators-B 9, 1992, pp. 63–69.

[10] P. Lv, Z.A. Tang, J. Yu, F.T. Zhang, G.F. Wei, Z.X. Huang, and Y. Hu. "Study on a micro-gas sensor with SnO2-NiO sensitive film for indoor formaldehyde detection," Sens. Actuators-B 132, 2008, pp. 54-80.

[11] H. Kudo, M. Sawai, Y. Suzuki, X. Wang, T. Gessei, D. Takahashi, T. Arakawa, and K. Mitsubayashi, "Fiber optic bio-sniffer (biochemical gas sensor) for high selective monitoring of ethanol vapor using 335 nm UV-LED," Sens. Actuator B-Chem, 147, 2010, pp. 676-680.

[12] Mitsubayashi K., Nishio G., Sawai M., Saito T., Kudo H., Saito H., Otsuka K., Noguer T., and Marty J-L., A bio-sniffer stick with FALDH (formaldehyde dehydrogenase) for convenient analysis of gaseous formaldehyde. Sens. Actuators B 130, 2008, pp. 32-37.

 ISBN: 978-1-61208-261-5

Steam Gasification of Coffee Husk in Bubbling Fluidized Bed Gasifier

Sileshi Kore, Abebayehu Assefa
Mechanical Engineering Department
Addis Ababa University
Addis Ababa, Ethiopia
e-mail: {sileshikore, abebayehuassefa}@yahoo.com

Mayerhofer Matthias, Hartmut Spliethoff
Institute of Energy System
Technical University of Munich
Munich, Germany
e-mail: {m.mayerhofer, splithoff}@tum.de

Abstract- **Currently, the worldwide demand for fossil fuel is increasing rapidly and, at the same time, known resources are diminishing. In particular, energy resources, such as oil and natural gas, are almost depleted in some parts of the world. In addition, the fact that the climate changes are more severe than before has increased the demand for renewable energy resources. Thus, energy from biomass is one of the potential renewable energy options. The availability of biomass, combined with the recent development of technologies to use it efficiently, with low level of emission, promise to make biomass an increasingly attractive fuel option. Coffee husk is an agricultural waste in coffee processing industries in different parts of Ethiopia that has the potential of exploiting energy via thermo-chemical conversion such as gasification. However, the characteristic properties of this material with regard to thermo-chemical conversion technologies are missing in literature. This study focuses on the experimental investigating of coffee husk in bubbling fluidized bed gasifier. The performance parameters that were investigated during the experiment were tar content and gas composition. The study findings show that the tar content of coffee husk gasification is not disturbing the smooth operation of the gasifier and the gas composition observed was good as compared to wood pellet. Therefore, coffee husk will be promising feedstock in fluidized bed gasification.**

Keywords-coffee husk; tar-content; gas composition; fluidized bed; gasification.

I. INTRODUCTION

As an agricultural country, Ethiopia produces considerable amount of biomass each year. Most of biomass has been utilized for domestic energy purpose, mainly by direct combustion (which converts solid biomass into heat). On the contrary, coffee husk from coffee processing industries is not used as a fuel in most cases due to the poor handling of coffee husk to be used as domestic fuel. However, gasification, which converts solid biomass into fuel gas containing CO and H_2 or so-called synthesis gas, has to be considered as a promising alternative owing to a number of advantages. In the southern part of Ethiopia almost 171,000 tons of processed coffee is supplied to the international market per year. During the process, more than 20,000 tons of residue coffee husk is disposed of. This represents a very good potential for biomass energy.

Apart from gasification for heat production, biomass gasification for electricity or combined heat and electricity production especially at small scales has drawn great attention as a more efficient and economical option compared to conventional combustion steam cycle in Thailand [1]. Unlike air gasification, steam gasification requires an external heat source if steam is used as a sole gasifying agent. Even though using a mixture of steam and air as a gasifying agent is common technology, in this experimental work, the air is used to facilitate the flow of coffee husk. In addition, it is assisted by gravity, since the feed is at the top of the gasifier. Also, the oxygen in the air will help to provide some amount of energy due to the exothermic nature of burning biomass. The elevated temperature will help in the de-volatilization process of biomass to produce various gases. Steam will react with carbon monoxide to produce hydrogen and carbon dioxide.

The coffee husk is processed in an atmospheric bubbling fluidized bed reactor. Because fluidized beds can handle a large variety of feedstocks, they are well suited for this application [2].

The motivation of this study is to investigate the extent to which the gas quality (tar and gas) can influence the operation of the gasifier using coffee husk as a feedstock as compared to that of wood pellet from published data at the same operating conditions.

The present work is organized as follows. The introduction part includes some overview of the availability of raw materials and available technologies to use coffee husk as renewable energy option. The methodology part describes experimental facilities and works that have been conducted at the Institute of Energy System, Technical University of Munich (IES TUM). In the result and discussion part, we present the findings of our experiments. Finally, conclusions are drawn.

Figure 1. Wood pellets

 ISBN: 978-1-61208-261-5

Figure 2. Coffee husks

II. METHODOLOGY

The study of biomass thermo-chemical conversion in fluidized bed reactors is among the most active research studies at the IES TUM. The in-house bubbling fluidized bed (BFB) facilities were developed and are located at the IES TUM as research test bench. The main biomass feedstock used is wood pellet (Figure 1.), which is generated from wood. In our work, coffee husk from coffee processing industries in Ethiopia is used to check whether coffee husk (Figure 2) is a promising biomass to be used in fluidized bed gasification. In addition to this, the institute is well equipped with regard to laboratory facility to analyze the thermo-chemical properties of biomass fuel, online product gas and FID to analyze tar material in the product gas (syngas).

The experimental study was performed in a bubbling fluidized bed (BFB) gasifier which is built at IES TUM. The reactor vessel is made of high temperature resistant steel (German material number 1.4841, AISI SS 310). The dimension of the reactor has an internal diameter of 154 mm and a length of 1.5 m and the schematic diagram of the gasifier is shown in Figure 3. The reactor can be operated up to 850 ^{O}C and pressurized up to 0.5 M Pa. The biomass is fed through a pressurized screw-conveyor into a drop shaft directly to the bottom of the bubbling fluidized bed gasifier. A small amount of air is flushed in to the biomass feeding system to sidestep the entrance of syngas or steam in the feeding system. The syngas as well as the steam flow to feed line should be prevented by all means as steam swells up the feedstock along the feed inlet pipe which leads quickly to obstruction of the feeding system. The bed has a height of approximately 700 mm and is fluidized using steam as fluidizing agent and gasification medium. The heat required for the endothermic gasification reactions is provided by electrical heating and transferred into the bed via four high temperature heat pipes which use sodium as a working fluid. The heat pipes have a diameter of 20 mm and a length of 660 mm inside the fluidized bed.

The heat pipes influence the flow dynamics to some extent and lead to the formation of a slug flow [3] throughout the whole height of the fluidized bed. All pipings are well insulated and the cyclone and the filter are heated up to a temperature of 330 ^{O}C to avoid tar condensation in order to mitigate condensed tar material, since condensed tar will disturb the operating condition of the gasifier. There are 15 thermocouples placed at equal distance along the direction of the reactor. The thermocouples are therefore bundled in a closed small steel tube that is introduced through the top flange of the reactor and sealed with a compression fitting.

The measurement procedure was as follows: the bed was heated up to the required temperature and fluidized with steam while the biomass feeding rate was set to achieve the steam to biomass set point. After observing a stable gas composition half an hour run, three tar samples were taken using the solid phase adsorption (SPA) method. The method uses solid phase extraction tubes filled with aminopropaylsiane phase bounded to silica gel. A detailed description of the SPA sampling and analysis method can be found in [4] Therefore, 100 ml of product gas was drawn with a syringe over an amino phase column. The results of the analysis are given with the assumption that the steam in the gas is condensed in the amino phase and does not enter the syringe in vapor form. This value was converted into g/m3 at standard conditions.

The selected operating temperature for coffee husk gasification in the fluidized bed gasifier was 800 ^{O}C. An increase in temperature will face ash sintering problem due to the coffee husk ash melting point which is around 815-820 ^{O}C. At the same time, lowering the gasification temperature will result in poor quality of the gasifier products. The selected operating parameters are indicated in Table I.

The synthesis gas (product gas) exits at the top of the reactor and is cleaned by passing the gas through a cyclone and a ceramic candle filter. Subsequently, the syngas is expanded in the pressure control valve to atmospheric pressure. At this point, the sample was taken to check the tar material. Finally, the gas was analyzed online for the main components H_2, CO, CO_2, and CH_4.

Silica sand (SiO_2) is used as a bed material in this experiment. The average particle size is 0.25 mm and minimum fluidization velocity is v_{mf} = 0.034 m/s. During this study the bed materials wed filled to the height of 0.39m of the reactor.

The feedstock characteristic of coffee husk was analyzed at the chemical laboratory which belongs to the IES, TUM. Therefore, Table II depicts the fuel characteristic of coffee husk. The study of thermo-chemical properties provides information about the quality of biomass material in terms of proximate and ultimate analyses, and heating values. The samples of coffee husks were taken from Gedeo zone, southern part of Ethiopia. Proximate analysis of biomass gives the weight fractions of volatiles, ash, and fixed carbon. The content of volatiles and ash has an influence on the thermo-chemical conversion, syngas composition and tar

 ISBN: 978-1-61208-261-5

materials. Ultimate analysis is carried out to determine the composition of hydrogen, carbon, nitrogen, oxygen and sulfur in a given biomass material. The heating value, also called calorific value or heat of combustion, defines the energy content of a given fuel. It is one of the most important parameters for design calculations and numerical simulations of thermal systems. The gasification products of a given biomass material are influenced by its thermo-chemical properties. The coffee husk size distribution was not uniform but less than 5mm. In the case of the wood pellet the size was uniform. Therefore, this step will incur some additional cost compared to coffee husk.

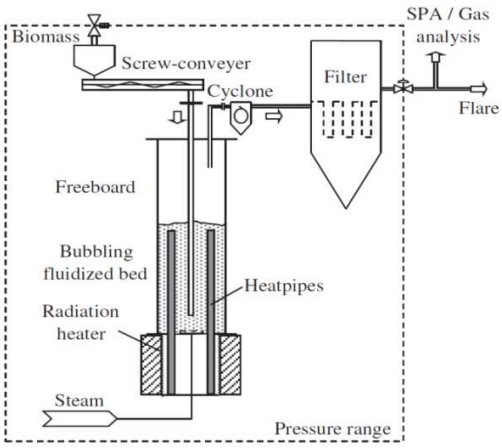

Fig.3 Schematic Diagram of the Bubbling Fluidized Bed Gasifier

TABLE I. OPERATING CONDITION OF BUBBLING FLUIDIZED BED GASIFIER

Properties	Operating Condition
Temperature (^{O}C)	800
Pressure	Atmospheric
Steam/biomass	0.83

TABLE II. COFFEE HUSK (GEDEO ZONE, ETHIOPIA) CHARACTERISTICS

Parameters	Values
Water content	8.36%
Lower heating value	17.2 MJ/kg
Proximate analysis (% wight dry basis)	
Ash content	6.99 wt. % db
Voletiles	72.30 wt. % db
Fixed carbon	20.71 wt. % db
Ultimate analysis (% weight, dry-ash-free basis)	
C	48.09 wt.% db
H	5.24 wt. % db
N	1.69 wt. % db
S	5.50 wt. % db
O	33.39 wt. % db

III. RESULT AND DISCUSSION

Three different tar samples are presented in Figure 4 to check whether or not the tar material affects the smooth operation of the gasification process. Generally, tars are hydrocarbon containing mixtures, which can form liquid or highly viscose to solid deposits by cooling of the gaseous phase down to ambient temperature. In addition to the main elements carbon (C) and hydrogen (H) other elements like oxygen (O), nitrogen (N) or sulfur (S) are found in tar. Tars are generally assumed to be largely aromatic [5]. Several researchers have worked on various tar classifications such as the division in primary, secondary and tertiary tar [6 - 8]. Tar materials from wood pellet can be referred to from the published data of Pletka et al. [2].

Over 800° C, tertiary tar can be found and tertiary tars are also called recombination or high temperature tars [9]. As the operating temperature of the test bench is at this temperature rage, most tar material in the analysis is tertiary tars. Figure 4 shows tar components in the product gas from coffee husk gasification. As the gasification process proceeds almost all tar contents are reduced. Thus, coffee husk gasification suffers little from tar challenge.

From the syngas evolution profiles presented, it can be seen that steam gasification consistently evolved major gas components H_2, CO, CO_2 and CH_4 with the respective percentages of 40%, 21%, 20% and 6%. Being combustible hydrogen, carbon monoxide and methane are desired component of the syngas whereas carbon dioxide is not desired as it plays a negative role on syngas heating value. The syngas heating value can be calculated based on these combustible gas components. Therefore, the syngas compositions are compared with wood-pellet gasification which is done in the same test bench and the same operation condition (pressure, temperature and steam to biomass ratio) from the published data [2].

 ISBN: 978-1-61208-261-5

Figure 5 shows the species from the gasification of wood pellet and coffee husk. From the bar-graph one can observe that CO, CO_2, CH_4 and H_2 compositions have no influential difference between the two feedstocks. Therefore, coffee husk is a good feedstock option for gasification in BFB gasifier.

Coffee husk gasification has dual advantage. The first advantage is economical advantage, since coffee husk should not be pelletized. Moreover, it is an agricultural residue from coffee husk processing industry (typically in the case of Ethiopia). The second advantage of using the feedstock will mitigate the environmental challenge arising from the dumping of the coffee husk to the environment by consuming this residue.

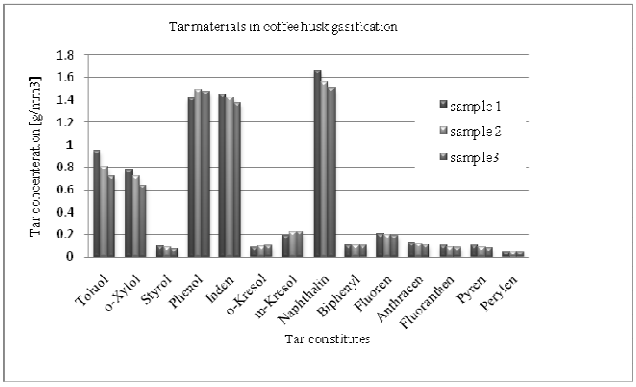

Figure 4. Tar compositions from coffee husk gasification

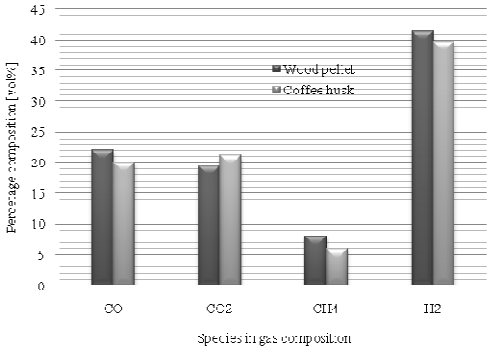

Figure 5. Species composition from wood pellet and coffee husk gasification

IV. CONCLUSION AND FUTURE WORKS

In this work, experimental results are reported regarding the influence of tar material in the smooth operation of the gasifier and gas composition during fluidized bed steam gasification using coffee husk as a feedstock.

The study findings show that the tar content of coffee husk can be gasified in bubbling fluidized bed without problems and the gas composition observed was good as compared to wood pellet. Therefore, coffee husk will be encouraging feedstock to be used in fluidized bed gasifier for biomass energy option.

Important future work will include performing experiments with various operating parameters.

REFERENCES

[1] P. Chobthiangtham, S. Pipatmanomai, "Co-Gasification of Biomass and Plastic Waste in a Bubbling Fluidized Bed Gasifier," Proceedings, World Renewable Energy Congress 2009 – Asia and The 3rd International Conference on Sustainable Energy and Environment (SEE 2009), 19-22 May 2009, Bangkok, Thailand.

[2] R. Pletka, R. Brown, and J. Smeenk, "Indirectly Heated Fluidized Bed Biomass Gasifier Using a Latent Heat Blast," Bioenergy '98 – Expanding Bioenergy Partnership, 8th biennial conference, Center for Coal and the Environment Iowa State University.

[3] M. Mayerhofer, P. Mitsakis, X. Meng, W. de Jong , H. Spliethoff , Gaderer M, "Influence of Pressure, Temperature and Steam on Tar and Gas in Allothermal Fluidized Bed Gasification,'' Fuel, vol. 99 Sep. 2012, pp. 204–209.

[4] C. Brage, Q. Yu, G. Chen, K. Sjöström."Use of amino phase adsorbent for biomass tar sampling and separation,'' Fuel, vol 76 1997, pp. 137–142.

[5] C. Unger, and M. Ising, "Mechanisms and significance of tar formation and tar removal in thermo-chemical conversion of solid carbon sources," German Society for Petroleum and Coal Science and Technology, Conference Report, Vol 2, 2002, pp. 131-142.

[6] T. Milne, R. Evans, and N. Abatzoglou, "Biomass Gasifier Tars: Their Nature, Formation, and Conversion," NREL, 1998.

[7] M. Kübel,"Tar formation and tar conversion in biomass gasification-Application of wet chemical tar intended to CEN standard," Goettingen: Cuvillier Publishing, 2007.

[8] J. Neeft, H. Knoef, and P. Onaji, Behavior of tar in biomass gasification systems -Tar related problems and their solutions, Utrecht: EWAB, 1999.

[9] I Aigner, U Wolfesberger, H. Hofbaue, "Tar Content and Composition in Producer Gas of Fluidized Bed Gasification and Low Temperature Pyrolysis of Straw and Wood –Influence of Temperature," Wien: Proceedings of the 1st International Conference on Poly-generation Strategies, 2009.

 ISBN: 978-1-61208-261-5

Green Growth and Sustainable Development

Monitoring Progress towards the Environmental Millennium Development Goals

Ana Jesús López Menéndez
Department of Applied Economics
University of Oviedo
Oviedo, Spain
anaj@uniovi.es

Rigoberto Pérez Suárez
Department of Applied Economics
University of Oviedo
Oviedo, Spain
rigo@uniovi.es

***Abstract*—According to the Organization for Economic Cooperation and Development (OECD), Green Growth means "Fostering economic growth and development, while ensuring that natural assets continue to provide the resources and environmental services on which our well-being relies". Furthermore, since Sustainable Development provides an important context for Green Growth, The United Nations Millennium Development Goals (MDG) include the goal "Ensure environmental sustainability", which considers four specific targets related to the development policies, the biodiversity loss, the proportion of people without access to safe drinking water and sanitation facilities and the improvement in the lives of slum dwellers. In this context, our paper aims to provide both analytical and empirical contributions for the monitoring of the MDG achievements. With this regard we firstly propose a Poverty-Growth-Environment triangle, and then we analyze the available statistical evidence in order to summarize the current progress and future perspectives towards the Environmental Millennium Development Goals.**

Keywords- MDG; growth; environment; poverty; EKC.

I. INTRODUCTION

The increasingly industrialized and interconnected world is experiencing harmful environmental changes, which could threaten future human wellbeing.

In this context, the Organization for Economic Cooperation and Development (OECD) has launched the Green Growth initiative, which –according to [1] – aims "Fostering economic growth and development, while ensuring that natural assets continue to provide the resources and environmental services on which our well-being relies".

Green growth can be considered as a subset of sustainable development, since it is narrower in scope, focusing on measurable progress at the interface of the economy and the environment.

Appropriate information and comparable data are required in order to track progress towards green growth, and with this aim, the OECD is exploring a list of suitable indicators, which should consistently combine economic and environmental information, leading to a System of Environmental and Economic Accounting (SEEA) which is currently in progress.

The challenge of ensuring environmental sustainability is also included in the United Nations Millennium Development Goals (MDG). More specifically, four different targets are specified within this goal, including a total of ten indicators, which allow monitoring the progress towards the environmental objectives.

In this paper we firstly describe the Poverty-Growth-Environment relationships and their connections with the environment targets included in the Millennium Development Goals.

Then, we focus on the available indicators in order to quantify progress towards these targets, also analyzing the regional disparities and testing for convergence.

Finally the paper ends with some concluding remarks and a list of the main bibliographical references.

II. GREEN GROWTH AND ENVIRONMENTAL MDG

The Millennium Development Goals (MDGs) provide a combination of human needs and basic rights that every individual around the world should be able to enjoy. More specifically, the United Nations Millennium Declaration adopted in the General Assembly Resolution 55/2 (year 2000) by 189 State Members established certain fundamental values including freedom, equality, solidarity, tolerance, respect for nature and shared responsibility, leading to a set of specific and measurable objectives known as the Millennium Development Goals (MDG) to be achieved by 2015.

The eight agreed goals are respectively referred to poverty, primary education, gender equality, child mortality, maternal health, diseases as AIDS and malaria, environmental sustainability and global partnership. In this paper we mainly focus on the seventh goal, described as "Integrate the principles of sustainable development into country policies and programs and reverse the loss of environmental resources", which includes four specific targets and a list of ten indicators, as summarized in Table I.

A detailed description of these indicators appears in [2].

The achievement of the Millennium Development Goals requires concrete strategies and special attention to the most vulnerable people, countries and regions. Therefore, we adopt the conceptual framework proposed by F. Bourguignon in his Poverty-Growth-Inequality triangle described in [3], assuming that "the rapid elimination of absolute poverty, under all forms, is a meaningful goal for development". Within this context, Figure 1 illustrates the

 ISBN: 978-1-61208-261-5

Poverty-Growth-Environment Triangle approach to the environmental MDG.

TABLE I. ENVIRONMENTAL MDG TARGETS AND INDICATORS

Targets	Indicators
7A: Integrate the principles of sustainable development into country policies and programs and reverse the loss of environmental resources 7B: Reduce biodiversity loss, achieving, by 2010, a significant reduction in the rate of loss	7.1 Proportion of Land Area covered by forest 7.2 CO2 emissions (total, per capita and per $1 GD, PPP) 7.3 Consumption of ozone-depleting substances 7.4 Proportion of fish stocks within safe biological limits 7.5 Proportion of total water resources used 7.6 Proportion of terrestrial and marine areas protected 7.7 Proportion of species threatened with extinction
7C: Halve, by 2015, the proportion of people without sustainable access to safe drinking water and basic sanitation	7.8 Proportion of population using an improved drinking water source 7.9 Proportion of population using an improved sanitation facility
7D: By 2020, to have achieved a significant improvement in the lives of at least 100 million slum dwellers	7.10 Proportion of urban population living in slums

Source: United Nations, Millennium Development Goals

More specifically, speaking in terms of the MDG targets, we should focus on halving by 2015 the proportion of people without sustainable access to safe drinking water and basic sanitation, and achieving by 2020 a significant improvement in the lives of slum dwellers. Both objectives are related to the Poverty vertex of the triangle.

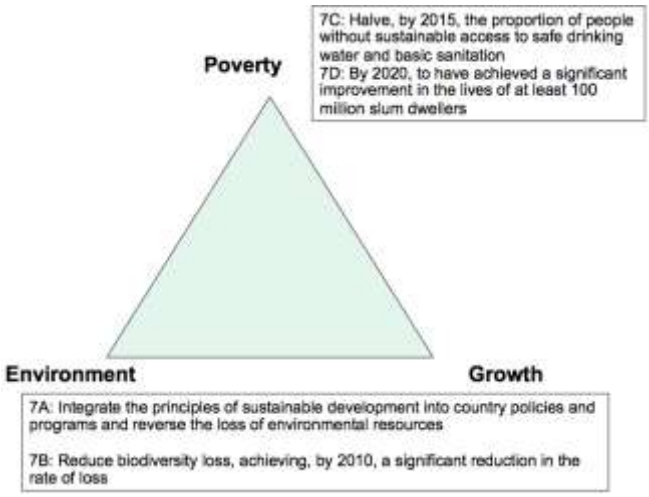

Figure 1. Poverty-Growth-Environment Triangle and Millennium Development Goals

In a second stage, a balance should be found between the objectives of growth and environment, whose relationships have been widely studied, leading to a controversial debate mainly focused on the Environmental Kuznets Curve (EKC).

Inspired in the inverted U-shaped relationship between inequality and per-capita income proposed by Simon Kuznets [4], the Environmental Kuznets Curve holds that environmental quality initially worsens with the increases in per-capita income, but then improves after an Income Turning Point (ITP).

Since a wide variety of empirical investigations regarding the EKC have been published during the last decades, some meta-analyses have been recently developed in [5] and [6]. As expected, results indicate that the estimated EKC-type relationships depend on several aspects as data characteristics, environmental indicators or methodological choices.

III. MONITORING PROGRESS TOWARDS THE MDG

Three years to the deadline, broad progress on the MDGs has been reported by United Nations [7], especially regarding the reduction of extreme poverty and the proportion of people without access to improved sources of water, and the improvement in the lives of slum dwellers. Nevertheless, achievements were unequally distributed across and within regions and countries. Moreover, progress has slowed for some MDGs after the international crisis, which has significantly impacted the economic perspectives thus affecting the odds of achieving the required targets.

With the aim of providing a more complete description of the progress towards the environmental goals during the last decades and the future perspectives for 2015 and beyond, in the next sections we present a spatial analysis based on the United Nations Database.

A. Poverty Targets

Since the poverty reduction should be considered a priority, we firstly focus on poverty indicators, which have shown a good behavior according to the 2012 Millennium Development Goals Report [7]. More specifically, preliminary estimates confirm that the first target of the MDGs (cutting the extreme poverty rate to halve by 2015 its 1990 level) will be achieved at the global level.

This report also emphasizes that number of people living in extreme poverty (with less than 1.25 dollars a day) and the corresponding poverty rates are falling in every developing region, including Sub Saharan Africa, where the figures are particularly higher.

Regarding the environmental goals, the reduction of poverty is the aim of targets 7C (halving the proportion of people without access to safe drinking water and basic sanitation) and 7D (achieving a significant improvement in the lives of at least 100 million slum dwellers). According to the 2012 MDG Report, the world has already met the target of halving the proportion of people without access to improved sources of water, and improvements have been

 ISBN: 978-1-61208-261-5

achieved in the lives of 200 million slum dwellers, thus exceeding target 7D.

In order to provide a more detailed analysis of these achievements we can compute a Performance Index, defined as:

$$I_t = \frac{X_t - X_{1990}}{X^* - X_{1990}} \quad (1)$$

where X_{1990}, X_t, X^* respectively denote the 1990 value, the current value and the proposed target. This index has been recently computed in [8], showing outstanding progress for poverty goals while the lowest levels correspond to AIDS spread, child mortality and access to primary education.

Table II summarizes the results obtained for target 7C, showing significant differences between regions (Eastern Asia shows the best behavior while the worst corresponds to Sub Saharan Africa) and also between indicators 7.8 and 7.9 (the progress achieved with regard to access to drinking water is higher than the improvement in sanitation facilities).

Furthermore, differences also exist between rural and urban areas (although this information is not collected in the table), being the rural performance higher than the urban indicator.

TABLE II. PERFORMANCE INDEX FOR TARGET 7C

Region	Performance Index	
	7.8 Population using an improved drinking water source	7.9 Population using an improved sanitation facility
World	1.08	0.55
Developing Regions	1.07	0.58
Northern Africa	0.77	1.29
SubSaharan Africa	0.47	0.11
Latin America & Caribbean	1.20	0.75
Eastern Asia	1.44	1.07
Southern Asia	1.29	0.45
South-Eastern Asia	1.17	0.85
Western Asia	0.53	0.50
Oceania	0.00	0.00

Source: Self elaboration using United Nations Database

Regarding target 7D, Figure 2 represents the proportion of urban population living in slums, showing a positive evolution with the exception of Western Asia, whose figure increases during the last decade. Nevertheless, the worst situation corresponds to Sub Saharan Africa, with more than 63% of its urban population living in slums.

On the opposite side, an outstanding improvement is found in Northern Africa, whose initial situation was similar to that of Latin America and Caribbean, but has gradually decreased leading to the lowest proportion of urban population living in slums. Positive behaviors are also found in Southern, Eastern and South-Eastern Asia, whose figures decreased significantly.

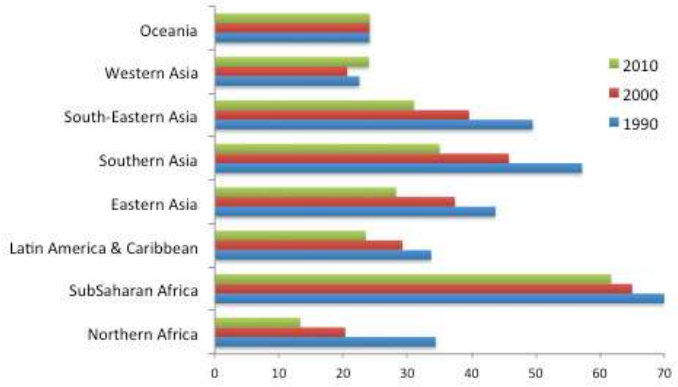

Figure 2. Proportion of urban population living in slums

B. *Environmental MGDs and regional convergence*

The previously proposed Performance index cannot be computed for most environmental goals, since they do not provide a specific target. Nevertheless, progress towards the MDGs can be approached through the cumulative growth rate, computed as:

$$r = \left(\frac{X_t}{X_{1990}} \right)^{\frac{1}{t-1990}} - 1 \quad (2)$$

Besides summarizing the MDG achievements, cumulative growth rates provide a useful tool in order to analyze regional disparities or test for convergence. Thus, table III summarizes the main regional results referred to eight different environmental targets (only 7.4: proportion of fish stocks within safe biological limits and 7.5: proportion of total water resources used, have been excluded due to the lack of information).

In general terms, the obtained results agree with the expected signs, leading to negative rates of growth for the proportion of species threatened with extinction (7.7), the proportion of urban population living in slums (7.10), and the consumption of ozone-depleting substances (7.3).

Table III also shows a parallelism in the behaviors of developing regions and the world as a whole. This fact is quite interesting and leads to the question of regional convergence.

Furthermore, as we have previously said, the achievement of the MDGs is particularly important for poor regions and countries, thus suggesting the need of testing for convergence. With this aim we have tested, for each of the considered indicators, if the cumulative rates of growth are inversely related with the initial registered values, referred to year 1990.

 ISBN: 978-1-61208-261-5

TABLE III. CUMULATIVE GROWTH RATE 1990-2010

Region	Environmental Indicator							
	7.1	**7.2**	**7.3**	**7.6**	**7.7**	**7.8**	**7.9**	**7.10**
World	-0.2	1.7	-8.5	2.0	-0.1	0.8	1.3	
Developing Regions	-0.3	3.2	-9.1	2.2	-0.1	1.0	2.0	-1,7
Northern Africa	0.0	1.8	-12.4	1.0	0.0	0.3	1.1	-4.6
SubSaharan Africa	-0.5	0.0	-12.5	0.4	0.0	1.1	0.7	-0.6
Latin America & Caribbean	-0.5	0.9	-12.3	3.9	-0.1	0.5	0.8	-1.8
Eastern Asia	1.1	4.5	-8.4	1.4	-0.1	1.5	4.6	-2.2
Southern Asia	0.1	3.6	-6.6	0.8	-0.1	1.1	2.7	-2.4
South-Eastern Asia	-0.7	3.8	-0.3	2.7	-0.1	1.1	2.1	-2.3
Western Asia	0.8	1.6	-5.0	7.3	0.0	0.2	0.3	0.3
Oceania	-0.4	0.2	-13.8	9.7	0.0	0.0	0.0	0.0

Source: Self elaboration using United Nations Database

The estimation results are summarized in Table IV, suggesting the existence of convergence only for some of the considered indicators.

More specifically, only two out of eight regressions lead to significant coefficients at the one percent level (related to indicators 7.3 and 7.8) while two more estimated coefficients result to be significant at the five percent level.

Nevertheless, we must stress that all the estimated coefficients, even when non-significant, show negative sign, thus excluding the existence of divergence.

TABLE IV. CONVERGENCE ANALYSIS

Indicator		
	Estimated slope	R squared
7.1 Proportion of Land Area covered by forest	-0.0001 (*)	0.13
7.2 CO2 emissions (per capita)	-0.003 (**)	0.28
7.3 Consumption of ozone-depleting substances	-0.0000002 (***)	0.58
7.6 Proportion of terrestrial and marine areas protected	-0.003	0.18
7.7 Proportion of species threatened with extinction	-0.00001	0.10
7.8 Proportion of population using an improved drinking water source	-0.00019 (**)	0.29
7.9 Proportion of population using an improved sanitation facility	-0.0003 (***)	0.56
7.10 Proportion of urban population living in slums	-0.0001	0.03

Source: Self elaboration using United Nations Database

* significant at 10% **significant at 5%; ***significant at 1%.

IV. CONCLUDING REMARKS

The Millennium Development Goals (MDGs) include the challenge of achieving environmental sustainability, specifying four targets referred to the development policies (7A), the biodiversity loss (7B), the proportion of people without access to safe drinking water and sanitation facilities (7C) and the improvement in the lives of slum dwellers (7D).

With the aim of monitoring the progress towards the environmental MDGs, we have assumed a Poverty-Growth-Environment framework, thus considering poverty (targets 7C and 7D) as a first priority, and then focusing on the growth-environment goals (targets 7A and 7B).

Following this approach and according to the available information, we can conclude that progress has been made during the last two decades, although significant disparities remain between different regions and targets.

Thus, our results confirm that Sub Saharan Africa performance is particularly poor for most of the considered indicators, while Eastern Asia performs quite well in most of the considered goals.

Regarding convergence, the regressions of the cumulative rates of growth on the initial values lead to negative estimated coefficients for all the considered indicators, but only half of them result to be significant at the 5% level.

ACKNOWLEDGMENT

The authors would like to acknowledge the support provided by the University of Oviedo through the Cluster of Energy, Environment and Climate Change (Campus of International Excellence "*Ad Futurum*").

REFERENCES

[1] OECD, Green Growth, Towards Green Growth, Paris, May 2011.

[2] United Nations, Indicators for Monitoring tth Millennium Development Goals, United Nations Development Program, New York, 2003.

[3] F. Bourguignon, "The Poverty-Growth-Inequality Triangle", Working Paper n 125, Indian Council for Research on International Economic Relations, New Delhi, 2004.

[4] S. Kuznets, "Economic Growth and Income Inequality", American Economic Review, vol. 49, 1955, pp. 1-28.

[5] B.S. Koirala, H- Li and R.P. Berrens, "Further Investigation of Environmental Kuznets Curve Studies using Meta-Analysis", Journal of Ecological Economics & Statistics, vol. 22, n. 11, 2011, pp. 13-32.

[6] B.R.Jordan, "The Environmental Kuznets Curve: Preliminary Meta-Analysis of Published Studies, 1995-2010", Georgia Tech School of Public Policy, Workshop on Original Policy Research (WOPR), December 2010.

[7] United Nations, The Millennium Development Goals Report, New York, 2012.

[8] A.J. López and R. Pérez, "Measuring Progress towards the Millennium Development Goals. A Regional Approach", ERSA Congress, Barcelona, August-September 2011.

[9] A.J. López and B. Moreno, "Renewable Energy in the European Union: An Econometric Approach to Trends and Effects" Biosciencesworld, The First International Conference on Biosciences, 2010, pp.95-98.

 ISBN: 978-1-61208-261-5

Torrefied Pellets As Fuel For Two-stage Technology Of Biomass Conversion Into Synthesis Gas

Victor Zaichenko, Valentin Kosov, Julia Kuzmina, Vladimir Lavrenov
Joint Institute for High Temperatures of the Russian Academy of Sciences (JIHT RAS),
Moscow, Russia
E-mails: zaitch@oivtran.ru, kosov@ihed.ras.ru, juli_kuzmina@mail.ru, v.a.lavrenov@gmail.com

***Abstract*— One of the most important properties of the torrefied pellets, along with high calorific value, is their hydrophobicity. Inability to absorb moisture and self-destruct under its influence determine possibility of using of pellets in the pyrolysis reactor. For the technology of two-stage thermal processing of biomass, developed at the Joint Institute for High Temperatures, the amount of synthesis gas which can be obtained from one kilogram of torrefied pellets is also important. A construction of the pilot torrefaction reactor powered by flue gas is shown. The results of experimental investigations of hydrophobicity of torrefied pellets produced by the reactor and quantity of synthesis gas which can be obtained by two-stage thermal processing of the pellets are presented. It is shown that torrefaction allows simplifying the process of conversion of pellets into synthesis gas without significant reduction in the volume of the gas.**

Keywords - biomass conversion; torrefaction; pyrolysis; syngas.

I. INTRODUCTION

The most effective way to convert biomass is its conversion into combustible gas. However, the existing conversion technologies of solid hydrocarbon raw materials in gaseous fuel have several disadvantages.

Air gasification is the easiest method to convert biomass into the gas. However, the resulting gas contains up to 60% nitrogen and 40% carbon dioxide. The calorific value of the gas is generally around 4 - 5 MJ/m^3, which is too low for efficient use. Overall efficiency of gasification gas power plant is limited to 20% [1].

Oxygen and steam gasification allow increasing the calorific value of the gas which contains no nitrogen and small amount of carbon dioxide. The maximum gas yield reaches 1.3 nm^3 per kg of raw material and its calorific value is about 11 MJ/m^3 [2]. Steam gasification is the widespread process because of its simplicity. The main disadvantage of the process is concerned with necessity of steam generation, which reduces overall effectiveness of power plant. Use of oxygen for the purpose of gasification demands an air separation unit in technological chain that leads to rise in price of end product. It should also be noted that purification of the gas from tar and ash is an urgent problem for all methods of gasification.

For several years, in the Joint Institute for High Temperatures of Russian Academy of Sciences, the two-stage technology of biomass processing has been developing [3, 4]. The technology is based on pyrolysis of biomass as the first stage. The second stage is high-temperature conversion of liquid fraction of the pyrolysis on the surface of porous charcoal matrix. Synthesis gas consisted from carbon monoxide and hydrogen is the main products of the technology.

Our experiments have shown a significant increase of the volume of gas in the outlet of the reactor due to decomposition of condensable and non-condensable pyrolysis products. In comparison to pyrolysis, the volume of gas increased nearly 10 times at cracking temperature 1000 ° C. At this temperature, the gas consists almost entirely of hydrogen and carbon monoxide in approximately equal parts in the zone of maximum gas release.

To implement this technology at the Joint Institute for High Temperatures, an experimental model of power station of electric power up to 5 kW was created. The power station consists of a thermochemical reactor, control and measurement system, and a gas-diesel engine with an electric generator.

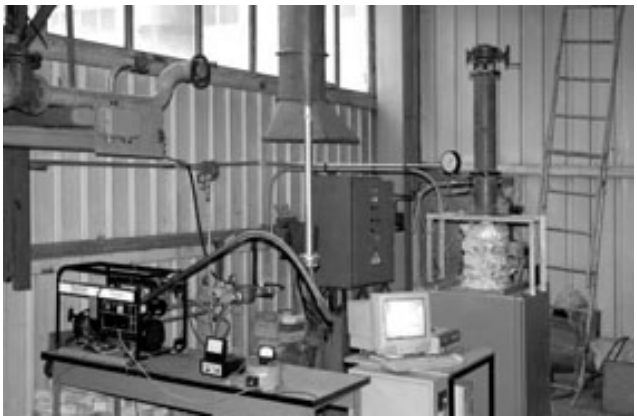

Figure 1. Experimental power station of electric power up to 5 kW.

During the test of the power station, a problem with the high hygroscopicity of wood pellets was detected. Pellets that are in the low-temperature zone of the reactor absorbed water vapor rising from the high-temperature zone. As a result of swelling of the pellets, the gas-tight stopper formed that blocked operation of the reactor. Preliminary drying of pellets allowed to improve the situation only insignificantly, but did not remove the main problem. To solve the problem,

 ISBN: 978-1-61208-261-5

it was suggested to use torrefied pellets as fuel for the thermochemical reactor.

The second section describes construction of the torrefaction reactor that was created in Joint Institute for High Temperatures of the Russian Academy of Sciences and characteristics of produced torrefied pellets. The third section describes the technology of two-stage thermal processing of biomass that use torrefied pellets as a raw material for synthesis gas production.

II. TORREFACTION REACTOR

It is known that torrefaction allows reducing substantially the ability of biomass to absorb the atmospheric moisture. During the torrefaction process biomass heated up to the temperature 250 – 270ºC, the moisture and quantity of the volatile matter leaves, in result calorific value of biomass increased from 19 to 22 MJ/kg and biomass gets waterproof properties.

To achieve these goals, the torrefaction reactor using as a heat source exhaust gases of power station engine was created. The reactor is shown at the Figure 2.

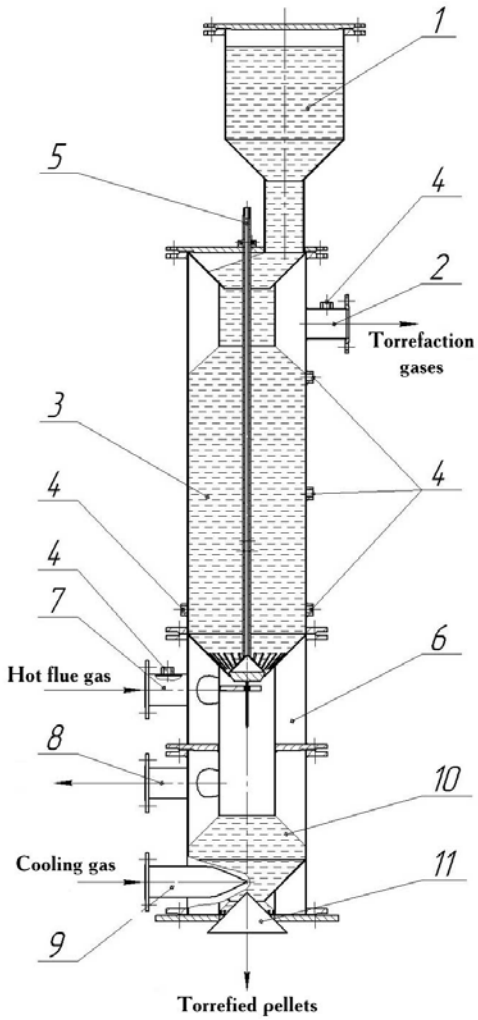

Figure 2. Torrefaction reactor

Raw material is loaded into the reactor through the feed tube 1 and fills the volume of the top of the reactor tank 3. Hot gases flow through the pipe 7 in average tank 6, passing through the perforated cone, heat pellets and leave through the pipe 2. The flow rate of the hot flue gases was 242.5 nm3 per hour. The temperature of the hot flue gases was regulated by temperature control system (is not shown at the Figure 2) consisted of a gas-water heat exchanger and a mixer.

With the rod 5 with closing sphere, the hot pellets are discharged into the lower tank 10, where they are cooled by cold gases. Cooled Pellets unloaded from the reactor when the cone-unloader is open.

The main feature of the proposed scheme is the use exhaust gas of the internal combustion engine as gas coolant. Thus, two problems are solved. Firstly, due to the high heat transfer coefficient an efficient heating processed raw material provides in comparison with schemes in which the heat input through the reactor wall. Secondly, the proposed scheme, in essence, is a co-generation unit which allows generating electricity and utilizing the heat produced by in order to improve the properties of the solid biomass fuel. This approach significantly improves the economics of the whole process of processing of pellets into synthesis gas.

For the purpose of using the obtained torrefied pellets as a fuel or raw material for further processing, it is important to know their properties of hygroscopicity and calorific value. Figure 3 shows the change of hygroscopicity of torrefied wood pellets obtained in the reactor at three temperatures of torrefaction 230°C, 250°C and 270°C, in comparison with original raw material. The total torrefaction time for all cases was 60 min.

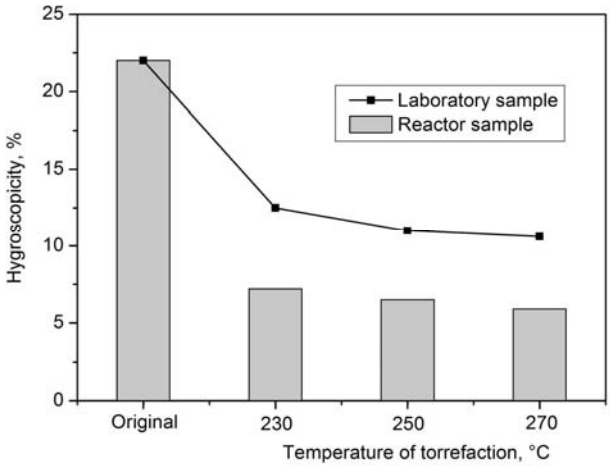

Figure 3. Hygroscopicity of wood pellets obtained in the torrefaction reactor in comparison with laboratory sample.

The figure also presents the values hygroscopicity of torrefied pellets obtained in the laboratory at the same temperatures. From the data above, it follows that hygroscopicity of the torrefied pellets is significantly lower than hygroscopicity of the original pellets. In this case, hygroscopicity of pellets obtained in the reactor even lower than that of laboratory samples. Long-term experiments

 ISBN: 978-1-61208-261-5

(about 72 hours) showed that the torrefied pellets are not destroyed under the influence of moisture and retain their structure.

The results of measurements of the relative increment of the calorific value of wood pellets in comparison to the original material are shown in the Figure 4. Calorific values of samples torrefied in the laboratory are shown as well.

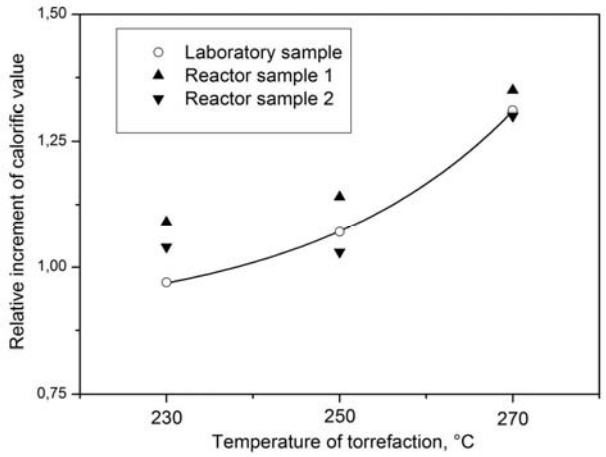

Figure 4. Relative increment of the calorific value of wood pellets obtained in the torrefaction reactor in comparison with laboratory sample.

From the data presented, it follows that pellets obtained in the torrefaction reactor have similar properties of calorific value as the laboratory samples. Small variations in the relative increment of the calorific value of pellets obtained in the torrefaction reactor can be explained by differences in the properties of the original material and the non-uniformity of the thermal field inside the reactor.

In general, it can be concluded that the proposed construction of the reactor allows obtaining torrefied pellets of high quality suitable for use as fuel and as raw material for further processing.

III. TWO-STAGE THERMAL PROCESSING OF TORREFIED WOOD PELLETS

The technology of biomass thermal processing with synthesis gas production developed in the JIHT RAS is based on high-temperature processing of the pyrolysis gases and volatiles. The method is similar to the one suggested in [5] and used in [3, 4] for processing of wood waste and peat. Products of biomass pyrolysis are char, non-condensable pyrolysis gases (CO_2, CO, H_2,) and liquid fraction. Carbon, hydrogen and oxygen content of condensable and non-condensable volatiles allows them to be converted into synthesis gas consists of hydrogen and carbon monoxide in practically equal parts.

During torrefaction some part of volatiles leave the biomass reducing the total amount of biomass synthesis gas that can be obtained from it and lowering the total effectiveness of the technology. It was important to determine the amount of synthesis gas that could be obtained from the torrefaction volatiles and compare it to the amount of gas is produced from torrefied pellets.

The experimental set-up (Figure 5) was similar to one described in [3] and consisted of a high-temperature two-chamber fixed-bed reactor and a system of extraction and analysis of gas and vapor forming as a result of heating an initial raw material.

The reactor was a stainless steel tube with an inside diameter of about 37 mm, which was placed within two-section furnace with independent heaters for each section. The chambers were 300 mm length each. Raw material was placed into the bottom chamber. Char obtained by pyrolysis of the same raw material was placed in the top chamber. The depth of char bed was equal to 50 mm. Before experiments the top chamber was heated up to temperature 1000°C that was held further at the constant level. After that the temperature of the bottom chamber was raised at the rate 10°C/min.

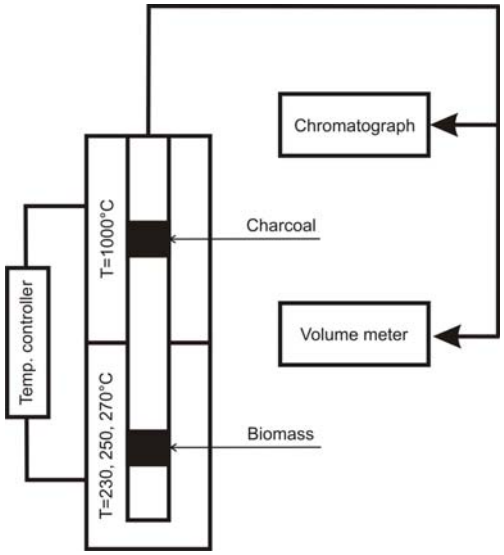

Figure 5. Scheme of the experimental reactor

Pyrolysis gases formed during pyrolysis of initial raw material passed through the porous carbon bed with the fixed temperature. As a result of homogeneous and heterogeneous chemical reactions in the high-temperature zone, a decomposition of torrefaction gases took place. Conversion degree depended both on the temperature in the top chamber and on the residence time in a high-temperature zone. Non-condensable gas came into the volume meter (eudiometer). The samples of the gas were chromatographed.

There were two series of experiments. In the first series of experiments the amount of synthesis gas that can be produced by thermal decomposition of volatiles formed during torrefaction was determined. In the second series of experiments, the amount of synthesis gas that can be produced by thermal decomposition of volatiles formed during pyrolysis of the preliminary torrefied pellets was determined. There were also carried out experiments on the

 ISBN: 978-1-61208-261-5

production of synthesis gas from the initial non-torrefied pellet.

The data on gas volume (per kg of initial raw materials) obtained in the process of wood pellets torrefaction at constant temperature of the top chamber are shown in Figure 6. It can be seen that high-temperature conversion of torrefaction volatiles allows obtaining from 0.2 м^3 to 0.3 м^3 of synthesis gas consisted from hydrogen and carbon monoxide in practically equal parts.

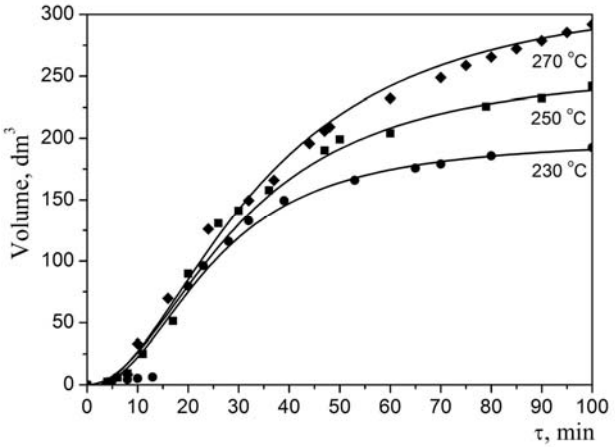

Figure 6. Gas yield per one kg of raw material during torrefaction of wood pellets.

Based on the material balance, it can be assumed that the decrease in the volume of gas produced from torrefied pellets will be less than gas volume produced from the initial non-torrefied pellets on a comparable value.

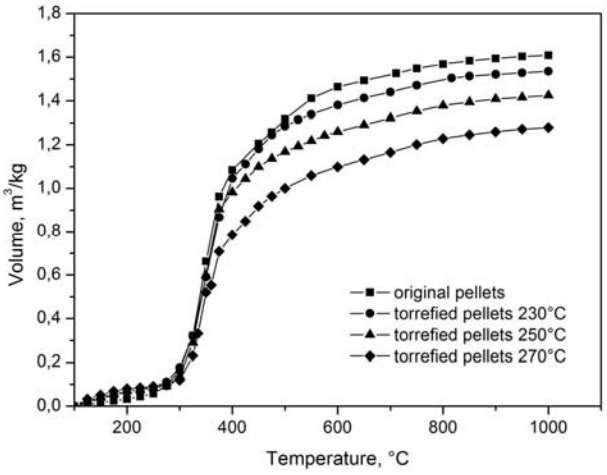

Figure 7. Gas yield per one kg of torrefied wood pellets during its thermal processing.

Experimental results on the two-stage thermal treatment of torrefied wood pellets into synthesis gas showed the validity of this assumption. Figure 7 shows the dynamics of the yield of synthesis gas during the thermal treatment of torrefied pellets. In this case the synthesis gas also consisted from hydrogen and carbon monoxide in practically equal parts. Reducing the amount of the resulting synthesis gas compared to initial raw pellets was from 0.1 м^3 to 0.3 м^3.

Thus, the inclusion in the technological scheme the torrefaction reactor for pretreatment of wood pellets allowed to solve the problem of the destruction the pellet during the pyrolysis process and did not significantly reduce the resulting volume of synthesis gas.

IV. CONCLUSION AND FUTURE WORK

Preliminary heat treatment of pellets from biomass can solve the problem of the destruction of moisture. Even the low-temperature torrefaction at 230°C allows reducing the hygroscopicity of wood pellets more than twice.

The proposed construction of the torrefaction reactor which is used as the heat source of gas-diesel exhaust gases provides production the torrefied pellets with desired properties. Hygroscopicity of wood pellets obtained from the reactor was lower than that of the sample obtained in the laboratory.

Increased calorific value of the torrefied wood pellets allows using them not only as raw material for a two-stage processing into synthesis gas, but also as a source of heat for ensuring thermal regime of the process.

Optimal mode of torrefaction of wood pellets is a low-temperature heat treatment at the temperature of 230°C that allows the process implementation without significant reduction in the volume of product gas.

Future work will include an elemental analysis of the biomass torrefied at different torrefaction temperature to determine the H/C and O/C ratio. Also it will be determined the energy balance for the technology.

REFERENCES

[1] M. Lisý, P. Kohout, Z. Skála, M. Balás, and J. Moskalík: Biomass Gasification and Cogeneration, 16th European Biomass Conference, (2008), pp. 843-849.

[2] L. Pengmei, Y. Zhenhong, M. Longlong, W. Chuangzhi, C. Yong, and Z. Jingxu: Hydrogen-rich gas production from biomass air and oxygen/steam gasification in a downdraft gasifier, Renewable energy, Vol. 32, no. 13, (2007), pp. 2173-2185.

[3] V.V. Kosov, V.F. Kosov, I.L. Maikov, V.A. Sinelshchikov, and V.M. Zaichenko. High calorific gas mixture produced by pyrolysis of wood and peat., The Proceedings of 17th European Biomass Conference and Exhibition, 29 June - 3 July 2009, Hamburg, Germany, pp. 1085 – 1088

[4] V.F. Kosov, V.A. Sinelshchikov, and V.M. Zaichenko. New Teechnology for Integrated Processing of Biomass and Natural Gas with Production of Hydrogen and Pure Carbon Materials, The Proceedings of 16th European Biomass Conference and Exhibition, Valencia, Spain, 2008, pp. 1171 – 1175.

[5] S.K. Chembukulam, A.S. Dandge, N.L. Kovilur, R.K. Seshagiri, and R. Vaidyeswaran, “Smokeless Fuel from Carbonized Sawdust”, Ind. Eng. Chem. Prod. Res. Dev., vol. 20, 1981, pp. 714-719.

 ISBN: 978-1-61208-261-5

Influence of Torrefaction on the Fuel Characteristics of Different Biomass Materials

Vladimir F. Kosov, Vladimir A. Sinelshchikov, George A. Sytchev, Victor M. Zaichenko
Joint Institute for High Temperatures of Russian Academy of Sciences
Moscow, Russia
e-mail: sinelshchikov@mail.ru

Abstract—**Possibilities of use of low-temperature pyrolysis (torrefaction) for improvement of heat engineering characteristics of biomass granulated fuel are considered. The data on hygroscopic properties, content of volatile matter and specific combustion heat of the torrefied fuel, produced under various conditions of processing of such types of biomass as wood, peat and agricultural waste, are presented. It is shown that the high-temperature conversion of gases and vapors, escaping during torrefaction, into synthesis gas is an effective method of their environmentally friendly utilization and, at the same time, increases the energy efficiency of biomass processing to granulated fuel.**

Keywords - biomass; solid fuel; torrefaction; pyrolysis; synthesis gas

I. INTRODUCTION

At present biomass are widely used in the power purposes. It is caused by development of self-sufficient power units, increasing attention to ecological aspects of warm and the electric power production, availability and renewable character of biomass as a fuel, tendency to energy safety of regions and countries. Methods of power utilization of biomass can be divided into two main groups, namely, direct use as a solid fuel and processing into gaseous or liquid fuel. In spite of distinctions in the properties of wood, agrowaste (sunflower and rice husk, straw) and peat, the production of granulated solid fuel (for example, pellets) from mentioned types of biomass obtains a wide spread occurrence. One of the main disadvantages of the granulated biomass fuel is bad hygroscopic property that complicates its storage and transportation and results in need to use of a moisture-proof package. Decrease in the hygroscopicity of biomass pellets can be achieved by their thermal processing. The thermal processing in the range of temperatures up to 300^{O}C, carried out in the inert gas environment (low-temperature pyrolysis), leads to an improvement of consumer properties of solid fuel from biomass. In scientific literature this process is known as a torrefaction and can be used both as a prior operation before pelletisation [1, 2], and as processing of the solid granulated (briquetted) fuel from biomass [3]. In course of torrefaction not only the moisture removal from an initial raw material, i.e. its drying, occurs but also partial thermal decomposition of an organic constituent of biomass takes place. As a result a solid hydrophobic product is formed. In addition its specific combustion value Q_t surpasses a similar value for initial raw material. In case of use of wood waste as initial raw material the value of Q_t can reach 19-23 MJ/kg depending on conditions at which the torrefaction is carried out [1]. Note that the combustion value of a dry wood and wood pellets doesn't exceed 18 MJ/kg. The present paper is devoted to investigation of influence of the torrefaction conditions on such properties of end product as devolatilization, specific combustion value and hygroscopicity.

II. EXPERIMENTAL CONDITIONS

As raw materials there were used such types of biomass as wood, straw and peat. Thermal processing of pellets from the mentioned biomass materials consisted in their heating in the inert gas environment (nitrogen) to the torrefaction temperature T_t = 230, 250 and 270^{O}C at the rate of 10^{O}C/min and holding at this temperature during some time.

When heating biomass there is its thermal decomposition and as a result a residual char and volatile products are formed. The volatile products consist of noncondensable gases, namely CO_2, CO, H_2, N_2 and C_nH_m (among gaseous hydrocarbons the basic is CH_4), and condensable gases and vapor forming the liquid fraction under the normal conditions. Composition of each fraction and a quantitative ratio between them depend both on the final temperature of heating and on the heating rate. The yield of volatile products defines the mass loss of a raw material during its thermal processing. For measurements of the quantitative characteristics concerned with mass loss of raw materials during heating the thermogravimetric analysis were carried out. For this purpose the thermogravimetric analyzer SDT Q600 was used. The SDT Q600 allowed also to make the differential calorimetric analysis and it was used during investigations of the influence of torrefaction on the combustion value of granulated biomass fuel.

III. RESULTS AND DISCUSSION

A. Torrefaction Process

Mass loss observed at the initial stage of heating (up to the temperature about 150^{O}C) is caused by release of physically bound water, i.e. drying of material, and characterizes its initial moisture content. In our case the moisture content of the samples was equal to 5.4% for wood pellets, 6.6% for peat pellets and 5.6% for straw pellets.

 ISBN: 978-1-61208-261-5

Further mass loss is caused by a thermal decomposition of organic constituent of raw material. Hydrocarbon raw materials of a phytogenesis consist of organic and mineral components. In turn organic part falls into hemicellulose, cellulose and lignin. Hemicellulose is the least thermostable organic component. According to [4] thermal decomposition of hemicellulose accompanied with mass losses occurs in the temperatures range of 200-270^{O}C (with maximum rate at 245^{O}C), cellulose – in the temperatures range of 280-370^{O}C (with maximum rate at 330-335^{O}C). Thermal decomposition of lignin follows more uniformly in comparison with two other components, and is characterized by a temperature interval 200-540^{O}C.

Time history of the mass loss rate of wood pellets during torrefaction is well seen from the differential thermogravimetric curves (DTG) presented in Fig. 1: the first peak characterizes the drying rate of the sample, the second peak – the rate of thermal decomposition of the material. The maximum rate of mass loss is observed when the sample temperature reaches the value of T_t whereupon the rate decreases because of reduction of sample mass. As appears from Fig. 1 in 100 minutes after the onset of heating the rate of mass loss falls off practically on an order of magnitude. Based on this fact during investigations of the influence of torrefaction on the thermotechnical characteristics of granulated fuel from biomass the time of thermal processing was limited by the specified value.

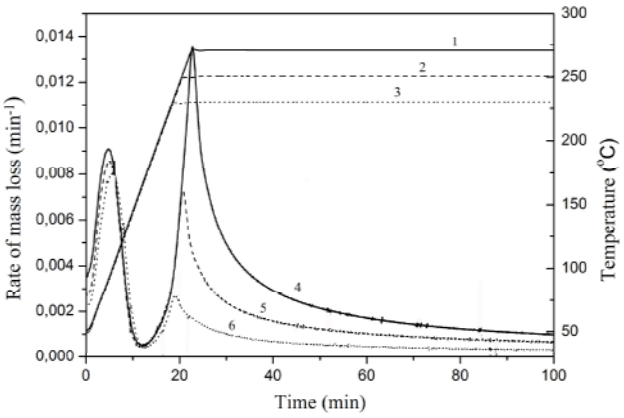

Figure 1. Change of temperature (1, 2, 3) and rate of mass loss (4, 5, 6) of wood pellets during torrefaction at T_t = 270^{O}C – 1, 4; 250^{O}C – 2, 5; 230^{O}C – 3, 6.

DTG curves describing dynamics of mass loss during pyrolysis (heating up to 1000^{O}C at the rate 10^{O}C/min) of the original and torrefied wood pellets are presented in Fig. 2. In DTG curve, corresponding to the original sample, one can see three representative knees (are marked by arrows) associated with thermal decomposition of hemicellulose, cellulose and lignin. In DTG curve, corresponding to the sample subjected to torrefaction at T_t = 270^{O}C, the knee attributed to thermal decomposition of hemicellulose disappears that is evidence of practically complete absence of it in the sample.

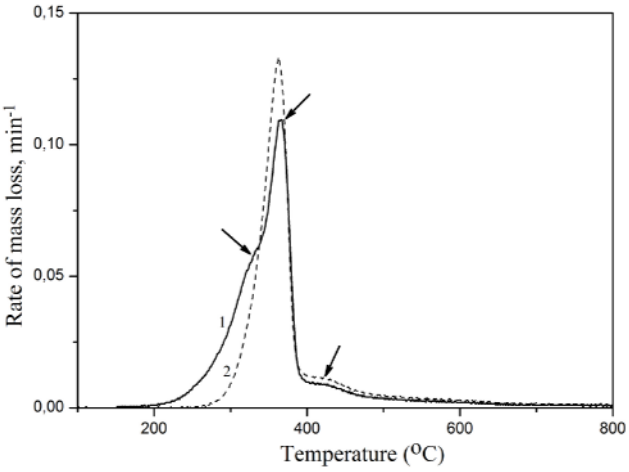

Figure 2. DTG curves of original wood pellets (1) and wood pellets torrefied at T_t = 270^{O}C (2) (heating rate -10^{O}C/min).

In Table 1 the data on mass loss for different types of initial raw materials as a result of torrefaction at different temperatures T_t are submitted. From these data one can see that the smallest mass loss at torrefaction is observed for wood pellets, the greatest – for pellets of straw that is mainly concerned with the various content of hemicellulose in these raw materials. Note, that the maximum mass loss, re-counted on a dry state, as a result of pyrolysis of initial raw materials (heating up to the temperature of 1000^{O}C) accounts for 82, 64, 72 % for pellets of wood, peat and straw, respectively.

TABLE I. MASS LOSS AS A RESULT OF TORREFACTION, RE-COUNTED ON DRY STATE (%)

Torrefaction Temperature, T_t (°C)	**Raw material**		
	Wood pellets	***Peat pellets***	***Straw pellets***
230	6.4	18	17
250	14	23	27
270	25	30	43

Decomposition of an organic part of a raw material, occurring during torrefaction, leads to change of its internal structure that is verified by electron micrographs. As a result of release of the volatile products the ratio between carbon, hydrogen and oxygen in a raw material changes that leads to change of its combustion value. Thus in consequence of torrefaction an initial raw material changes the thermotechnical properties, important at its use as a solid fuel.

B. Devolatilization

The ratio between the content of volatile and solid matters in a solid fuel has essentially influence on process of its burning. In particular, the rate of combustion is generally

 ISBN: 978-1-61208-261-5

defined by the rate of combustion of a solid carbon residue. Solid carbon residue makes main contribution to the combustion value of solid fuel also. In Table 2 the data on content of volatile matter in the initial raw materials and in the raw materials torrefied at different temperatures are submitted. From the presented data it follows that an increase in the torrefaction temperature T_t leads to a decrease of the content of volatile matter and, therefore, to an increase of mass fraction of solid carbon residue. The greatest difference between initial and torrefied raw materials is observed for pellets of straw. It is necessary to note that decrease of the volatile matter content leads to decrease of soot content in combustion products of a solid fuel. Soot is formed as a result of thermal decomposition of hydrocarbon components contained in the volatile products and responsible for smoke emission.

TABLE II. MASS FRACTION OF THE VOLATILE MATTER IN THE INITIAL AND TORREFIED RAW MATERIALS, RE-COUNTED ON DRY STATE (%)

Torrefaction Temperature, T_t (°C)	**Raw material**		
	Wood pellets	***Peat pellets***	***Straw pellets***
230	81	60	66
250	79	57	62
270	76	53	51
Starting state of raw material	82	64	72

C. *Hygroscopicity and Combustion Value*

Other important properties characterizing a solid fuel are the combustion value Q and the limit moisture content W. In Fig. 3 and 4 there are shown the data on influence of the torrefaction temperature T_t on the above-mentioned properties. The limit moisture content W was measured as the ratio of the equilibrium mass of water retained by a material in the air with 100% humidity at the temperature of 26°C to the mass of dry material.

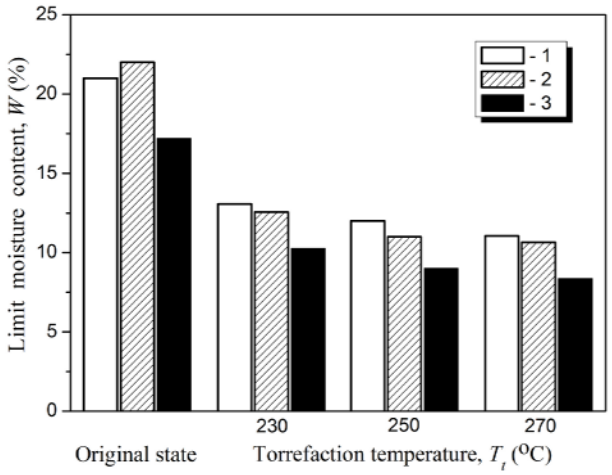

Figure 3. Effect of torrefaction temperature T_t on limit moisture content W for pellets of straw – 1, wood – 2 and peat – 3.

From the data presented in Fig. 3 one can see that the torrefaction allows essentially to improve the hygroscopic property of granulated fuel of the different biomass materials: the limit moisture content of pellets torrefied at T_t = 270°C halves practically in comparison with untreated pellets. It is necessary to note, that untreated wood pellets swelled and collapsed after holding during 24 hours in the air with 100% humidity at the temperature of 26°C. The torrefied wood pellets kept the form in the similar conditions.

In Fig. 4 there are shown the data on influence of torrefaction on the combustion value of pellets from different biomass materials. From the presented data it follows that an increase of torrefaction temperature results in appreciable increase of specific combustion value. The maximum growth is observed for peat pellets.

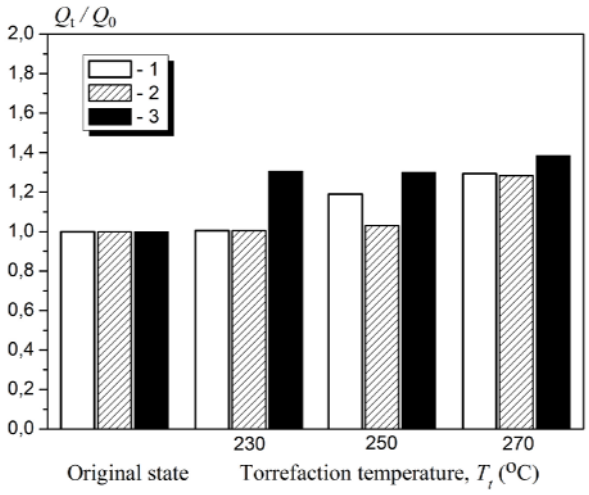

Figure 4. Effect of torrefaction temperature T_t on the ratio of combustion value of torrefied pellets Q_t to combustion value of original pellets Q_0 (re-counted on dry state): pellets of straw – 1, wood – 2 and peat – 3.

IV. CONVERSION OF VOLATILE TORREFACTION PRODUCTS INTO SYNTHESIS GAS

In torrefaction of a biomass the perceptible amounts of volatile products is evolved (see Table 1). Usually the mass fraction of condensable volatiles is several times as much as noncondensable one. According to [5] the condensable fraction of volatile products consists mainly of acetic acid and water with modest quantities of methanol, formic acid, lactic acid, furfural and hydroxyl acetone. It is natural that the question of their utilization is very important from the ecological point of view. For this purpose the technology of thermal conversion of pyrolysis gases and vapour, suggested in [6] and considered in [7] as applied to torrefaction, can be used. In conformity with this technology, the volatile products forming during heating the treated organic raw materials are filtered through a porous carbon medium maintained at a constant temperature. The coal residue obtained by pyrolysis (heating in the inert gas environment up to the temperatures of 600-1000°C) of the same raw material can be used as a porous carbon material. Owing to

 ISBN: 978-1-61208-261-5

its well-developed surface, a rapid heating of volatile products and intensive decomposition of the high-molecular organic components entering into their composition take place. In addition as a result of interaction of water vapor and carbon dioxide with a carbon surface a formation of hydrogen and carbon monoxide (the water gas reaction) and reduction of carbon dioxide to carbon monoxide (the Boudouard reaction) occur. At the temperature of the carbon medium about 1000^{O}C and suitable time of interaction of volatile products with a carbon surface practically complete conversion of the last into synthesis gas, i.e. a mixture of hydrogen and carbon monoxide, takes place.

In Fig. 5 there are presented the data on the volume content of hydrogen and carbon monoxide in gas mixture, which can be obtained as a result of high-temperature conversion of the volatile products forming during torrefaction of various biomass materials. Note that admixture of other gases, from which the basic is carbon dioxide, doesn't exceed 10 % (by volume).

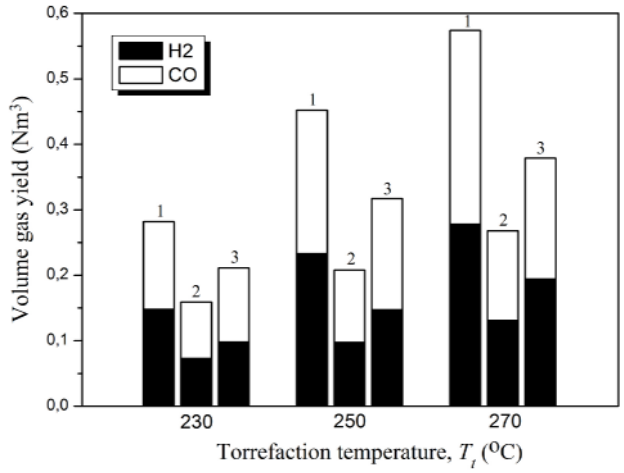

Figure 5. Volume yield of hydrogen and carbon monoxide per one kg of initial raw material vs. torrefaction temperature T_t for pellets from: straw – 1, wood – 2 and peat – 3.

The combustion value of the product synthesis gas is about of 11 MJ/m^3 that allows to consider it, as a quite acceptable gaseous fuel for power installations based on gas-piston engines. Let an average efficiency of transformation for electrogenerating installations on the basis of gas-piston engine is equal to 30 %, and the volume yield of the synthesis gas, which can be produced by high-temperature processing of the volatile products formed as a result of torrefaction of 100 kg of pellets, ranges between 20 and 55 m^3, depending on types of raw material and torrefaction temperature (see Fig. 5). In this case the use of the synthesis gas, produced on torrefaction of 100 kg of pellets per hour, will permit to maintain an electrogenerating installation with power of 18-50 kW in operation. At the same time the electrical power of plant for wood pellitization with productivity of 100 kg per hour doesn't exceed 7,5 kW and with a large supply can be provided at the expense of thermal processing of the torrefaction volatile products into synthesis gas.

V. CONCLUSION

As a result of performed experimental investigations it is shown that thermal processing of the granulated fuel from different biomass materials (wood, peat, straw) allows to improve its consumer properties, namely, to reduce the limit moisture content practically in half and to increase the specific combustion value noticeably. The volatile products obtained in the course of torrefaction can be converted into synthesis gas that allows to solve the problem of their utilization and simultaneously to increase the power efficiency of biomass processing. The considered approach can be used during engineering and creation of self-contained plants working directly in places of biomass production and intended for processing of different biomass materials (wood and agricultural waste, peat) into the granulated solid fuel with improved consumer properties and.

REFERENCES

[1] P. C. A. Bergman, “Combined torrefaction and pelletisation – the TOP process”, ECN Report, ECN-C–05-073. 2005, pp. 1–29.

[2] P. C. A. Bergman and J. H. A. Kiel, “Torrefaction for biomass upgrading”, ECN Report, ECN-RX–05-180. 2005, pp. 1–8.

[3] F. F. Felfi, C. A. Luengo, J. A. Suarez, and P.A. Beaton, “Wood briquette torrefaction”, Energy and Sustainable Development, vol. IX, 2005, pp. 19–22.

[4] A.N. Kislizyn, “Pyrolysis drevesiny: himizm, kinetika, producty, novie processy”, Lesnay promyshlennost, Moscow, 1990 (in Russian).

[5] M. J. Prins, K. J. Ptasinski, and J. J. G. Janssen Frans, “Torrefaction of wood. Part 2. Analysis of products”, J. Anal. Appl. Pyrolysis, vol. 77, 2006. pp. 35-40.

[6] V. M. Batenin, V. M. Zaichenko, V.F. Kosov, and V. A. Sinel’shchikov, “Pyrolitic Conversion of Biomass to Gaseous Fuel”, Doklady Chemistry, vol. 446, part 1, 2012, pp. 196–199.

[7] V. V. Kosov , V.F. Kosov, V.A. Sinelshchikov, and V. M. Zaichenko, “Torrefaction and Synthesis Gas Production”, The Proceedings of 19th European Biomass Conference and Exhibition, June 2011, Berlin, Germany, pp. 2011– 2014.

 ISBN: 978-1-61208-261-5

The Theoretical Research of Torrefaction Process in a Flow Reactor

Valentin Kosov, Igor Maikov, Natalya Medvetskaya, Oleg Stonyk
Joint Institute for High Temperatures of the Russian Academy of Sciences (JIHT RAS),
Moscow, Russia
E-mails: kosov@ihed.ras.ru, maikov_i@mail.ru, natalia-medvetskaya@rambler.ru, puma@oivtran.ru

***Abstract* — The processes of heat and mass transfer, such as drying, pyrolysis and heating of biomass particles during torrefaction in a flow reactor are considered. It is shown that for small particle size (~ 1 cm) heat transfer between the heating flow and the particles does not depend on mass transfer and the characteristic time torrefaction determined by the pyrolysis of biomass particles. Analytical dependences of concentration of the waste component of pellets under the condition of small time of heating and evaporation in comparison to the time of pyrolysis are made.**

Keywords— pellets; torrefaction; pyrolysis

I. INTRODUCTION

The processes of heat and mass transfer in porous medium are determining in many devices of chemical and energy industries. But despite the wide industrial application of porous materials, their uniform description is extremely difficult [1]. Most often some guesses based on experimental data for a specific process are used. Mass transfer and heat transfer are usually considered separately. Especially difficult to describe the processes in materials in which heat transfer is not only correlated with the mass transfer, but also changes the structure of the material. This also applies to torrefaction of organic substances which decompose when heated, and its different have different speeds of pyrolysis.

Torrefaction is the process of thermal processing of chopped or granulated biomass at temperatures up to 300 °C. Torrefaction is not only removing of moisture, i.e. drying of raw materials, but also thermal degradation of hemicellulose, which is part of the biomass. Typically, the process of torrefaction is described for a single sample biomass whether wood chips or pellets [2,3]. Description of this process most often based on a macroscopic energy considerations [4].

In this paper the mutual influence of heat and mass transfer (drying, pyrolysis, heating pellets) between pellets and hot gas stream during torrefaction of biomass in a flow reactor is considered. The existing experimental data for the coefficients of heat and mass transfer is involved.

II. INFLUENCE OF PYROLISYS ON HEATING OF PELLETS

The heat equation for a single pellet is:

$$\left[(1-\varepsilon)\rho_s c_{ps} + \varepsilon\rho_v c_{pv}\right]\frac{\partial T_s}{\partial t} = \Delta T_s - L\rho_i k_i e^{-\frac{E_i}{RT_s}} \qquad (1)$$

Indexes s and v refer to the solid skeleton and the pore space respectively, ρ - density, c_p - specific heat at constant pressure, T - temperature, ε - porosity, Δ - Laplacian. The last member corresponds to the pyrolysis of the core and the yield to the gas phase the exhaust components (we denote their accessories by index *i*) with the specific heat of phase transformation L and the activation energy $E \gg RT_s$.

If we represent the last member in (1) in the form of the time derivative of the weight loss, it is easy to estimate:

$$(1-\varepsilon)\rho_s c_{ps} \gg L\rho_i k_i \frac{E_i}{RT_s^2} e^{-\frac{E_i}{RT_s}} \qquad (2)$$

Specific numerical data were taken from [5].

Thus, to determine the temperature in the pellet it can be neglected the heat losses for outgoing components in comparison with the heat to heating of the pellet.

A similar estimate can be made regarding the impact of the gaseous products of pyrolysis of pellets on the density and velocity of the heating gas flow. Indeed, in a unit volume of pellet bed per unit time weight released

$$\sim 6(1-\varepsilon)/dke^{-\frac{E_i}{RT_s}},$$

where d is the diameter of the pellet. This value is several orders of magnitude less than the density of the gas stream which means that changing the velocity and density of the heating flow can be neglected.

If there is water in the pores it is necessary to consider its evaporation. We assume that water evaporation takes place at temperature of 100°C. Then the motion of the evaporation surface of radius r_0 deep into the particle radius R is given by:

$$\varepsilon\rho_l L\xi\frac{dr_0}{dt} = \frac{\lambda\Delta T}{r_0(1-r_0/R)} \qquad (3)$$

where λ - thermal conductivity of the dry core, ρ_l - water density, L - its boiling heat, ξ - its mass concentration in the pores which in normal conditions is not more than 10%, ΔT - temperature difference between the surface of the pellet and the evaporation temperature.

In equation (3), it was taken into account that the rate of evaporation is small in comparison to the speed of vapor movement through the pores, as density of bound water is much higher than vapor density.

Solving (2), we find that at temperature of 150 ÷ 180 °C for 3.3 ÷ 2.8 min. the pellets will be completely dried up from the pore water. As shown below, the temperature difference correspons to the temperature of the gas flow

 ISBN: 978-1-61208-261-5

and is set in a time much shorter than the time of pyrolysis. Thus, drying pellets is much faster pyrolysis processes.

III. HEATING OF PELLETS

Let us consider the temperature field in the pellet having size of about a centimeter. Its Fourier number has the following order [5]:

$$Fo = \frac{at}{R^2} \cong 0.13t \ , \qquad (4)$$

where a - thermal diffusivity, R - radius of the pellet, t-time in seconds.

Solution of the problem of thermal conduction in the sphere for a given surface temperature T_R and different numbers of Fourier is shown in Figure 1 [6]. It is easy to see that after 3 - 4 seconds the temperature field in the particle will actually homogeneous. For processes that are tens minutes last to neglect four seconds is acceptable. Note that this applies to the vapor diffusion in the pores.

The estimates give reason to believe that the heat exchange between the heating flow and pellets is independent of the mass transfer and the temperature distribution in the pellets is uniform.

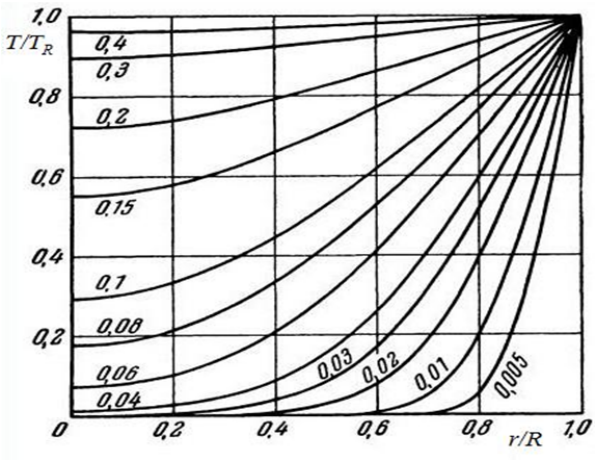

Figure 1. The temperature distribution in the sphere at different times. The numbers on the curves indicate the number of Fourier.

Heat exchange between the gas flow and the pellets that have the same effective diameter d and porosity ε_m is described by the following equations:

$$\frac{\partial \theta_f}{\partial \tau} + \frac{\partial \theta_f}{\partial z} = a(\theta_s - \theta_f) \qquad (5)$$

$$\frac{\partial \theta_s}{\partial \tau} = \theta_f - \theta_s \qquad (6)$$

where $\theta_f = \left(T_f - T_{s0}\right)/\left(T_{f0} - T_{s0}\right)$ and $\theta_s = (T_s - T_{s0})/\left(T_{f0} - T_{s0}\right)$ are dimensionless temperatures of flow and pellets respectively (the index 0 refers to the initial values),

$a = \left((1-\varepsilon_m)\left[(1-\varepsilon)\rho_s c_{ps} + \varepsilon\rho_v c_{pv}\right]\right)/\left(\varepsilon_m \rho_f c_{pf}\right)$,

$\tau = \alpha_T t/(1-\varepsilon_m)\left[(1-\varepsilon)\rho_s c_{ps} + \varepsilon\rho_v c_{pv}\right]$ is dimensionless time, $z = \tau x/u$ – dimensionless spatial coordinate; indexes f, s and v refer to the flow, hard core of pellets and its porous volume respectively, u – average velocity of the flow, α_T – heat transfer coefficient between the flow and the pellets [7]:

$$\alpha_T = 2.74\lambda(1-\varepsilon_m)^{1.36}\varepsilon_m^{-1} Re^{0.64} Pr^{1/3}/d^2 \qquad (7)$$

where the Re – Reynolds number: $30 < Re < 8 \cdot 10^4$; Pr – Prandtl number.

The initial and boundary values for the system (5), (6): $\theta_{s0} = 0, \theta_{f0}(z=0,\tau) = 1, \theta_{f0}(z,\tau=0) = 1$.

At fixed flow temperature pellets will have a temperature:

$$\theta_s = \theta_f(1 - \exp(-\tau)) \qquad (8)$$

When substituting the characteristic parameters in (7) (mean flow velocity u = 0.5 m / s) after 5 second the pellets temperature will be different from the flow temperature by ~ 2%.

But at the entry to the pellet layer the flow temperature is fixed, so the initial temperature difference at the entrance will be quickly leveled and the flow will not lost temperature on heating already heated pellets, i.e. heat wave will run by layer. The velocity, with which it will be distributed, can be obtained as follows. For the temperature difference we have solution [8]:

$$\theta_f - \theta_s = \exp(-\xi - \eta)\, I_0\left(\sqrt{2\xi\eta}\right) \qquad (9)$$

where I_0 is modified Bessel function, $\xi = za, \eta = \tau - z$.

Function $I_0\left(\sqrt{2\xi\eta}\right)$ has maximum at $\xi = \eta$, i.e. at $za = \tau - z$. But a is a big value, so $\approx \tau$. Considering what is z and τ, we obtain the maximum propagation velocity of the temperature difference:

$$U = u/a \qquad (10)$$

For the conditions under consideration, it is ~ 0.33 cm/s, i.e. by meter-thick layer of heating wave will run for about 5 minutes. We emphasize that this is exactly a wave, as if there was a zero right-hand side of (5), the left-hand side is exactly the wave equation. But, as we have shown previously, in our case the initial temperature difference quickly vanishes.

Thus, it can be argued that under these conditions the pellet heating is much faster than its pyrolysis, and thus, pyrolysis can be viewed at a specific temperature.

 ISBN: 978-1-61208-261-5

IV. CONCENTRATION OF EXHAUST COMPONENTS IN THE PELLETS.

Experimental data on the change in the total mass of pellets summarizes the various dependencies:

$$\frac{1}{m_0}\frac{\partial m_i}{\partial t} = -\left(\frac{m_i}{m_0}\right)^n k_i(T_s) \qquad (11)$$

where $k_i(T_s) = A_i exp(-E_i/RT_s)$ is the pyrolysis constant, A_i is the preexponential factor, E_i is the activation energy, m_0 and m_i are initial and current mass of the pellet, n is the reaction order, which is usually equal to 1, but for example in [9] it is equal to 1.8. If the current mass of the exhaust components in the solid skeleton is m_i, then its concentration $(x_i = m_i/m)$ satisfies the following equation:

$$\frac{\partial x_i}{\partial t} = -\left(\frac{m_i}{m_0}\right)^{n-1} k_i(T_s) x_i(1 - x_i) \qquad (12)$$

The solution of (11), (12) at a fixed temperature is trivial. Figure 2 shows the mass concentration of the volatiles of the flow at different temperatures (initial concentration 0.3,E_i= 220 kJ/mol, A_i = $2 \cdot 10^{17}$1/c, n =1.8 [9]).

The figure illustrates the strong dependence of the evolution of pellets composition on the temperature of the flow.

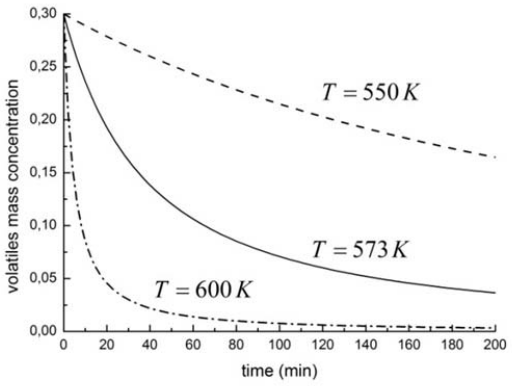

Figure 2. The time dependence of the mass concentration of the exhaust components at different gas temperatures.

V. CONCLUSION

It is shown that pellets are heated to the temperature of the gas flow is much faster than its pyrolysis proceeds. This applies to the initial pellets pore water evaporation. It can be assumed that the pyrolysis process most of the time takes place at a constant temperature equal to the temperature of the gas flow. The characteristic time of torrefaction is determined by the pyrolysis of biomass. We emphasize that this result relates to the small size of pellets (~ 1 cm).

REFERENCES

[1] I. Yasuaki and A.P.S. Selvadurai. Transport Phenomena in Porous Media. 2012.

[2] Y.Haseli, J.A. van Oijen, and L.P.H. de Goey, Predicting the pyrolysis of single biomass particles based on a time and space integral metod, Journal of Analytical and Applied Pyrolysis, vol. 96, March 2012, pp. 126–138, doi:10.1016/j.jaap., 2012.03.014.

[3] V. Repellin, A. Govin, M. Rolland, and R. Guyonnet, Modelling anhydrous weight loss of wood chips during torrefaction in a pilot kiln, Biomass & Bioenergy., vol. 34(5), January 2010, pp. 602 – 609.

[4] J. S. Tumurulu, S. Sokhansanj, C. Wright, and R.D. Boardman, Biomass Torrefaction Process Review and Moving Bed Torrefaction System Model Development, Idaho National Laboratory, Oak Ridge National Laboratory, 2010.

[5] W.-C.R. Chan, M. Kelbon, and B.B. Krieger, Modeling and experimental verification of physical and chemical processes during pyrolysis of a large biomass particle, Fuel,vol. 64, November 1985,pp. 1505 – 1513.

[6] H.S. Carslaw, J.C. Jaeger, Conduction of heat in solids, 2nd ed. Oxford: Clarendon Press, 1959.

[7] E.V. Venecianov, R.N. Rubinshtein, Dinamika sorbcii iz zhidkih sred, Moskva: Nauka, 1983 (in Russian).

[8] E.P. Serov, B.P. Korolkov, Dinamika processov v teplo- i massoobmennyh apparatah, Moskva: Energiya, 1967 (in Russian).

[9] T. Kashiwagi, H. Nambu, Global Kinetic Constants for Thermal Oxidative Degradation of a Cellulosic Paper, Combustion and Flame, vol. 88. March 1992, pp. 345 – 368.

 ISBN: 978-1-61208-261-5